Title

Multi-omics analysis of sarcospan overexpression in mdx skeletal muscle reveals compensatory remodeling of cytoskeleton-matrix interactions that promote mechanotransduction pathways

Journal

Skeletal Muscle, 13(1)

ISSN

2044-5040

Authors

McCourt, Jackie L
Stearns-Reider, Kristen M
Mamsa, Hafsa
et al.

Publication Date

2023

DOI

10.1186/s13395-022-00311-x

Peer reviewed

Skeletal Muscle

RESEARCH

Open Access

Multi-omics analysis of sarcospan overexpression in *mdx* skeletal muscle reveals compensatory remodeling of cytoskeleton-matrix interactions that promote mechanotransduction pathways

Jackie L. McCourt[1†], Kristen M. Stearns-Reider[1,2†], Hafsa Mamsa[1†], Pranav Kannan[1], Mohammad Hossein Afsharinia[1], Cynthia Shu[1], Elizabeth M. Gibbs[1], Kara M. Shin[1], Yerbol Z. Kurmangaliyev[3], Lauren R. Schmitt[4], Kirk C. Hansen[4] and Rachelle H. Crosbie[1,5,6,7*]

Abstract

Background The dystrophin-glycoprotein complex (DGC) is a critical adhesion complex of the muscle cell membrane, providing a mechanical link between the extracellular matrix (ECM) and the cortical cytoskeleton that stabilizes the sarcolemma during repeated muscle contractions. One integral component of the DGC is the transmembrane protein, sarcospan (SSPN). Overexpression of SSPN in the skeletal muscle of *mdx* mice (murine model of DMD) restores muscle fiber attachment to the ECM in part through an associated increase in utrophin and integrin adhesion complexes at the cell membrane, protecting the muscle from contraction-induced injury. In this study, we utilized transcriptomic and ECM protein-optimized proteomics data sets from wild-type, *mdx*, and *mdx* transgenic (mdx^{TG}) skeletal muscle tissues to identify pathways and proteins driving the compensatory action of SSPN overexpression.

Methods The tibialis anterior and quadriceps muscles were isolated from wild-type, *mdx*, and mdx^{TG} mice and subjected to bulk RNA-Seq and global proteomics analysis using methods to enhance capture of ECM proteins. Data sets were further analyzed through the ingenuity pathway analysis (QIAGEN) and integrative gene set enrichment to identify candidate networks, signaling pathways, and upstream regulators.

Results Through our multi-omics approach, we identified 3 classes of differentially expressed genes and proteins in mdx^{TG} muscle, including those that were (1) unrestored (significantly different from wild type, but not from *mdx*), (2) restored (significantly different from *mdx*, but not from wild type), and (3) compensatory (significantly different from both wild type and *mdx*). We identified signaling pathways that may contribute to the rescue phenotype, most notably cytoskeleton and ECM organization pathways. ECM-optimized proteomics revealed an increased abundance of collagens II, V, and XI, along with β-spectrin in mdx^{TG} samples. Using ingenuity pathway analysis, we identified

[†]Jackie L. McCourt, Kristen M. Stearns-Reider, and Hafsa Mamsa contributed equally.

*Correspondence:
Rachelle H. Crosbie
rcrosbie@physci.ucla.edu
Full list of author information is available at the end of the article

upstream regulators that are computationally predicted to drive compensatory changes, revealing a possible mechanism of SSPN rescue through a rewiring of cell-ECM bidirectional communication. We found that SSPN overexpression results in upregulation of key signaling molecules associated with regulation of cytoskeleton organization and mechanotransduction, including Yap1, Sox9, Rho, RAC, and Wnt.

Conclusions Our findings indicate that SSPN overexpression rescues dystrophin deficiency partially through mechanotransduction signaling cascades mediated through components of the ECM and the cortical cytoskeleton.

Keywords Duchenne muscular dystrophy, Dystrophin, Dystroglycan, Extracellular matrix, Sarcospan

Background

Duchenne muscular dystrophy (DMD) is a progressive muscle wasting disorder caused by mutations in the *DMD* gene encoding the protein dystrophin [1]. While dystrophin is expressed in multiple tissues, loss of dystrophin in the context of DMD is particularly detrimental to skeletal and cardiac muscle function [2]. Dystrophin is a component of the dystrophin-glycoprotein complex (DGC) that stabilizes the muscle fiber sarcolemma and mediates the linkage between the extracellular matrix (ECM) and the intracellular actin cytoskeleton [3–6]. Loss of dystrophin in DMD results in the absence of the DGC, destabilizing the sarcolemma and rendering it susceptible to contraction-induced damage [7]. Over time, chronic injury caused by asynchronous cycles of myofiber degeneration and regeneration results in failed muscle regeneration, inflammation, and replacement of functional muscle fibers with fibrosis [8]. Patients with DMD present with high plasma levels of muscle creatine kinase at birth, muscle fibrosis and hypertrophy, weakness of the proximal muscles, loss of ambulation, and pulmonary and cardiac dysfunction leading to premature death in the 2nd to 3rd decade of life [9–11]. While there are some FDA-approved treatment options for DMD, including corticosteroids and exon-skipping drugs that slow progression of the disease, there is still no cure.

The dystrophin-deficient *mdx* mouse is the most widely used mouse model for DMD as it exhibits much of the pathology observed in patient skeletal muscle, albeit much milder, including elevated creatine kinase levels, increased levels of degeneration and regeneration, fibrosis, and reduced grip strength and whole-body tension [12, 13]. While many therapeutic genes that improve sarcolemma instability, decrease fibrosis, and increase force in *mdx* muscle have been identified [14–21], there are gaps in understanding whether their protective mechanisms affect overlapping molecular processes and signaling pathways. Furthermore, there is emerging evidence of an expanded network of DGC-interacting proteins, suggesting that it functions as a central unit to integrate cellular signaling, lateral force transmission, ion channel function, and cytoskeletal organization [22, 23].

Sarcospan (SSPN), a core component of the DGC [24–26], prevents muscle degeneration and histopathology in *mdx* mice in a mechanism that is dependent on increased abundance of utrophin and integrin α7β1 at the sarcolemma [27–32]. Together with the sarcoglycans (SG), SSPN forms a tight subcomplex [26] that anchors α-dystroglycan, a receptor for many ECM proteins [33], to the cell membrane to stabilize the cytoskeleton-matrix linkage [34]. SSPN increases SG protein levels and restores integrity of the SG-SSPN subcomplex at the sarcolemma in *mdx* skeletal and cardiac muscles [27–31, 35]. SSPN overexpression in *mdx* mice also increased abundance of dystroglycan, enhanced matriglycan glycosylation of *α*-dystroglycan, and improved laminin binding [27, 30, 35, 36]. Using genetic approaches, we previously demonstrated that SSPN function is dependent on matriglycan modification of α-dystroglycan, which directly interacts with laminin [35]. Restoration of cell-matrix interactions by SSPN improved postexercise activity, protected against eccentric contraction-induced force loss, and prevented declines in pulmonary and cardiac functions [29–31].

In the current study, we interrogated the effects of SSPN overexpression on the *mdx* transcriptome and proteome using transgenic mouse models (Supplemental Table 1). Our findings build on many prior studies including microarray data sets (Omnibus GSE465, GSE1004, and GSE1007) [37] and proteomic analysis [37–44] of *mdx* muscle and DMD patient muscle biopsies, which revealed signaling pathways that contribute to the dystrophic pathology including anaerobic metabolism, cytoskeleton remodeling, calcium handling, adipogenesis, fibrosis, and endoplasmic reticulum stress. Given that there are many emerging approaches to treating DMD (dystrophin dependent as well as dystrophin independent), determining the effects of such treatments on cellular and molecular processes is important for therapeutic design. Such studies also have the potential to reveal overlapping pathways that are critical for prevention of muscle degeneration as well as pathways that are unaltered by a particular therapy (thereby informing molecular processes that are not major contributors to pathology). For instance, therapeutic restoration

of dystrophin expression in *mdx* muscle by antisense oligonucleotide exon skipping normalizes protein and mRNA expression toward wild-type levels, but does not affect the expression of microRNAs [37]. In our study, we found that SSPN overexpression in *mdx* muscle does not restore all transcripts and proteins to wild-type levels but ameliorates muscle pathology through compensatory changes in ECM and cytoskeletal composition, including key signaling molecules associated with regulation of cytoskeleton organization and mechanotransduction.

Methods

Mouse models

Wild-type (C57BL/6J) and *mdx* mice were purchased from Jackson Laboratories (Bar Harbor, ME, USA). We have generated and extensively characterized multiple lines of SSPN-transgenic *mdx* mice expressing either human SSPN (hSSPN, line 3, approximately 3-fold expression) [35] or murine SSPN (mSSPN, line 28, approximately 30-fold expression) [30] that are outlined in Supplementary Table 1. The SSPN transgenes were all under the control of the human skeletal α-actin promoter. hSSPN and mSSPN exhibit a high degree of identity (> 85%) at the amino acid level, effectively ameliorate *mdx* pathology, and were included in the study with the rationale that overlapping findings from different transgenic lines would strengthen their relevance. All mouse colonies were granted by the UCLA Animal Welfare Assurance (approval no. A3196-01).

Poly-A-enriched RNA sequencing

Liquid nitrogen frozen tibialis anterior muscles from 12-week-old male wild-type, *mdx*, and mdx^{TG} (line 28) were pulverized in a mortar and pestle cooled by liquid nitrogen and homogenized into TRIzol (Thermo Fisher Scientific, Waltham, MA, USA) using syringe homogenization with a 21g needle. RNA was extracted using TRIzol phase separation followed by QIAGEN RNeasy column purification using the manufacturer's instructions (QIAGEN, Hilden, Germany), followed by DNase treatment. RNA concentration and quality were measured using the TapeStation 4200 (Agilent Technologies, Santa Clara, CA, USA). RNA-Seq libraries were prepared from total RNA using the TruSeq Stranded mRNA Library Prep Kit (Illumina, San Diego, CA, USA). High-throughput sequencing was performed at UCLA Technology Center for Genomics & Bioinformatics using the Illumina HiSeq 4000 platform (paired-end 75 bp reads). Demultiplexing was performed with Illumina Bcl2fastq2 v 2.17 program. The total numbers of sequenced reads were 53–67 million per sample. RNA-Seq reads were mapped to the mouse reference genome (mm10) using STAR [45]. For each sample, 86% of reads were uniquely mapped to the genome. Expression levels were quantified for annotated genes (Ensembl v.92), and raw gene counts were normalized to CPM values (counts per million). The analysis was focused on genes with CPM > 1 in at least two samples (13,846 genes). Differential expression analysis was performed using edgeR-QLF [46]. Differentially expressed genes (DEGs) were identified at 1% FDR and fold-change > 2.

Mass spectrometry

The mass spectrometry dataset was first published in part in Stearns-Reider et al. [47]. Quadricep muscles were harvested from 20-week-old male wild-type, *mdx*, and mdx^{TG} (line 3) mice and snap frozen in liquid nitrogen. Samples were then prepared for mass spectrometry analysis as previously described [48]. In short, samples were pulverized in liquid nitrogen and lyophilized. For each sample, 5 mg (dry weight) of tissue was homogenized in 200 mL/mg high-salt buffer (HS buffer) containing a 1× protease inhibitor [48]. Following three rounds of HS buffer wash, pellets were treated with 6 M guanidine extraction buffer. The remaining pellets from each tissue, representing insoluble ECM proteins, were digested with freshly prepared hydroxylamine buffer, as previously described [49]. A total of 100 µl of the cellular fraction (combined fractions 1, 2, and 3) and 200 µl of the soluble and insoluble ECM fractions were enzymatically digested with trypsin using a filter-aided sample prep approach and C18 tip cleanup. Samples were then analyzed by liquid chromatography-data-dependent acquisition tandem mass spectrometry (LC-MS/MS), as previously described [50]. Samples were analyzed on a Q Exactive HF Orbitrap mass spectrometer (Thermo Fisher Scientific) coupled to an EASY-nanoLC 1000 system through a nanoelectrospray source. The analytical column (100 µm i.d. × 150 mm fused silica capillary packed in house with 4 µm 80 Å Synergi Hydro C18 resin (Phenomenex; Torrance, CA, USA)) was then switched online at 600 nL/min for 10 min to load the sample. The flow rate was adjusted to 400 nL/min, and peptides were separated over a 120-min linear gradient of 2–40% ACN with 0.1% FA. Data acquisition was performed using the instrument supplied Xcalibur (Thermo Fisher Scientific, San Jose, CA, USA) software in positive ion mode. MS/MS spectra were extracted from raw data files and converted into mgf files using a PAVA script (University of California, San Francisco, MSF, San Francisco, CA, USA). These mgf files were then independently searched against mouse Swiss-Prot database using an in-house Mascot server (version 2.2.06; Matrix Science, London, UK). Mass tolerances were +/−10 ppm for MS peaks and +/−0.5 D for MS/MS fragment ions. Trypsin specificity was used allowing for one missed cleavage. Met oxidation, pro-oxidation,

protein N-terminal acetylation, and peptide N-terminal pyroglutamic acid formation were allowed for variable modifications, whereas carbamidomethyl of Cys was set as a fixed modification. Following Mascot searches, data was directly loaded into Scaffold™ (Proteome Software Inc.). Peptide spectral matches were directly exported with a 99% confidence in protein identifications and at least 2 unique peptides per protein, resulting in a false discovery rate of 0.54%. Two-group comparisons were done by two-tailed Student's *t*-tests. Partial least squares-discriminant analysis (PLSDA) was performed using MetaboAnalyst (version 3.0) with sum and range scaling normalizations.

Indirect immunofluorescence staining of muscle sections

Transverse cryosections (10 μm) from the quadriceps muscles of wild-type, *mdx*, and *mdx*^{TG} (line 3) mice at 3–5 months of age were incubated in blocking buffer (3% BSA in phosphate-buffered saline (PBS)) for 30 min at room temperature. Avidin/biotin blocking kit (Vector Laboratories, Newark, CA, USA) was used according to manufacturer's instructions. Sections were then incubated with the following primary antibodies diluted 1:200 in PBS overnight at 4 °C: *β*-spectrin non-erythrocyte (PA5-52970, Thermo Fisher Scientific, Waltham, MA, USA), collagen type II (ab34712, Abcam, Waltham, MA, USA), and collagen type V (ab7046, Abcam, Waltham, MA, USA). Yap1 primary antibody (nb110-58358, Novus Biologicals, Centennial, CO, USA) was diluted 1:250. Sox9 antibody (AB5535, Sigma, St. Louis, MO, USA) was diluted 1:100. Sections were washed in PBS for 3 × 30 min at room temperature. Primary antibodies were detected by biotinylated anti-rabbit (BA-1000; 1:500; Vector Laboratories, Newark, CA, USA). Fluorescein-conjugated avidin D (A-2001; 1:500; Vector Laboratories) was used to detect secondary antibodies. Sections were mounted in Vectashield (Vector Laboratories, Newark, CA, USA), and imaging was performed using a Zeiss Axio Imager M2 (Carl Zeiss Inc., Thornwood, NY, USA) with a Hamamatsu ORCA-Flash 4.0 V3 digital complementary metal oxide semiconductor camera and a plan-Apochromat 20×/0.8 M27 objective. Percent nuclear Yap1 was quantified by counting Yap1-positive nuclei, with clear Yap1/DAPI overlap, divided by total DAPI content in five 20× fields per view per biological sample. Quantification of immunofluorescence analysis was performed on 20× images using ImageJ software (NIH, version 1.50i) for collagen II, collagen V, and *β*-spectrin by line scan analysis and Sox9 by measuring the integrated intensity in 4–12 images per genotype. For line scan measurements, using the line drawing tool on ImageJ, 40 areas of interest per biological replicate were quantified. Lines were drawn along or perpendicular to positive-stained areas, and peak intensity values were plotted denoted as "max" measurement on ImageJ.

Gene ontology and ingenuity pathway analysis

Gene ontology (GO) enrichment analysis for RNA sequencing and proteomic data sets was performed using the PANTHER classification system online user interface [51] and the statistical overrepresentation test. Fold enrichment values and *p*-values from the overrepresentation test were plotted using GraphPad Prism. RNA sequencing and proteomic data sets were also analyzed through the use of ingenuity pathway analysis (QIAGEN) for generating networks and upstream regulators [52]. Upstream regulators were sorted by activation score, and the top five inhibited and activated regulators were reported with corresponding target genes identified in the data sets.

Integrated gene set enrichment analysis

Significantly differentially expressed transcripts and proteins between *mdx* and *mdx*^{TG} were pooled as input for integrated gene set enrichment analysis using Database for Annotation, Visualization and Integrated Discovery (DAVID, version 2021). Each molecule was categorized as unrestored (significantly different from wild type, not significantly different from *mdx*), restored (significantly different from *mdx*, not significantly different from wild type), or compensatory (significantly different from both wild type and *mdx*). Data were visualized on Cytoscape version 3.9.1.

Supplementary figure methods

For a systems level network analysis, DEGs from the three identified categories (restored, unrestored, compensatory) were analyzed using the Database for Annotation, Visualization and Integrated Discovery platform (DAVID, version 2021). This analysis was also performed with the proteomic data set. Gene Ontology (GO) terms with corresponding parameter thresholds of $p < 0.05$ and minimum gene count = 2 were used as input and visualization in Cytoscape with the EnrichmentMap plugin.

Results

Gene expression and proteomic analyses reveal compensatory and restored pathways

In the current study, our goal was to interrogate the effects of SSPN overexpression on gene and protein expression in *mdx* muscle relative to wild-type and *mdx* (non-transgenic) controls. Gene expression analysis was performed using traditional poly-A-enriched RNA sequencing of tibialis anterior muscles isolated from 12-week-old wild-type, *mdx*, and *mdx*^{TG} mice. Principal component analysis of the sequencing data reveals clear

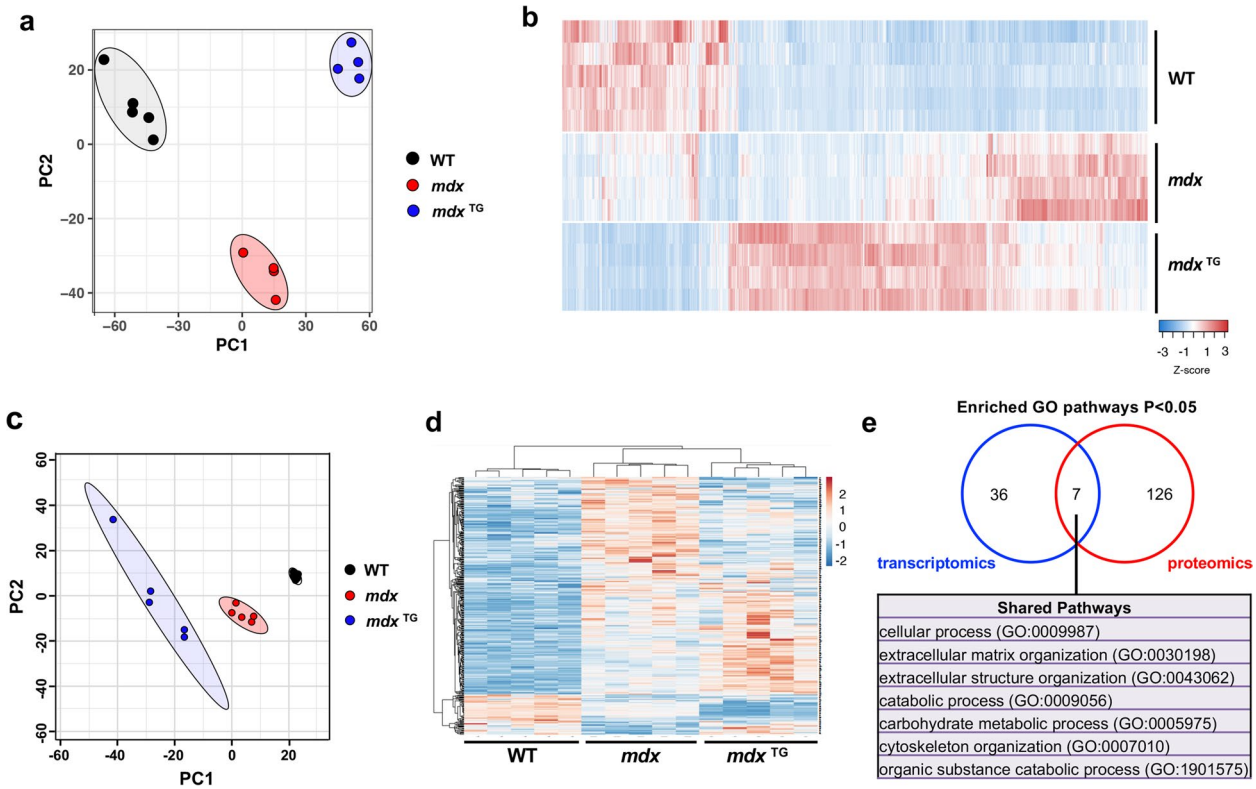

Fig. 1 Overview of RNA sequencing and mass spectrometry reveals distinct transcriptomic and proteomic profiles of SSPN overexpression rescue. **a** Principal component analysis (PCA) of RNA sequencing data in wild type (WT, $n = 5$), *mdx* ($n = 4$), and mSSPN transgenic (mdx^{TG}, $n = 4$) tibialis anterior muscle at 12 weeks of age. **b** Heat map of DEGs. **c** PCA of mass spectrometry data from WT ($n = 5$), *mdx* ($n = 5$), and hSSPN transgenic (mdx^{TG}, $n = 5$) quadriceps muscle at 20 weeks of age. **d** Heat map of differentially expressed proteins (DEPs). **e** Overlap of Gene Ontology (GO) terms enriched in WT vs mdx^{TG} in transcriptomics vs proteomics data using PANTHER GO analysis platform

clustering of each genotype (Fig. 1a). In comparing paired genotypes, we identified 1073 DEGs (853 upregulated, 220 downregulated) in wild-type versus *mdx* muscle and 748 DEGs (471 upregulated, 277 downregulated) in *mdx* relative to mdx^{TG} samples. The largest difference in the transcriptomic profile was evident between wild type and mdx^{TG} with 1857 DEGs (1306 upregulated, 551 downregulated). Heat map analysis of DEGs in mdx^{TG} relative to controls (Fig. 1b) reveals patterns that can be categorized as follows: (1) unrestored (significantly different from wild type, not significantly different from *mdx*), (2) restored (significantly different from *mdx*, not significantly different from wild type), and (3) compensatory (significantly different from both wild type and *mdx*).

Given the effects of SSPN overexpression on DEGs, we next investigated the influence of SSPN on protein expression utilizing a mass spectrometry approach that improves capture of typically insoluble ECM proteins [47, 53]. From our proteomics analysis of wild-type, *mdx*, and mdx^{TG} quadriceps muscle, we identified a total of 1679 proteins in all three genotypes. Principal component analysis revealed distinct clustering of the wild-type, *mdx*, and mdx^{TG} samples (Fig. 1c). Similar to the RNA sequencing data, we found sets of proteins in restored, unrestored, and compensatory categories (Fig. 1d).

Pathway enrichment analysis identifies compensatory changes in fibrillar collagens and components of the actin cytoskeleton

Comparative analysis of enriched GO pathways in the transcriptomic and proteomics data sets revealed seven shared pathways, including those associated with ECM organization, extracellular structure organization, and cytoskeleton organization (Fig. 1e). By separating enriched GO pathways into the compensatory, restored, and unrestored subcategories for both transcriptomic and proteomic data sets, we observed additional pathways of interest such as those associated with calcium ion binding, NAD/NADP binding, ubiquitin ligase binding, and oxidoreductase binding (Supplementary Fig. 1). Given the identification of the broader categories of ECM organization and cytoskeleton organization identified in the mdx^{TG} model through GO pathway analysis, we curated lists of actin cytoskeleton- and ECM-associated

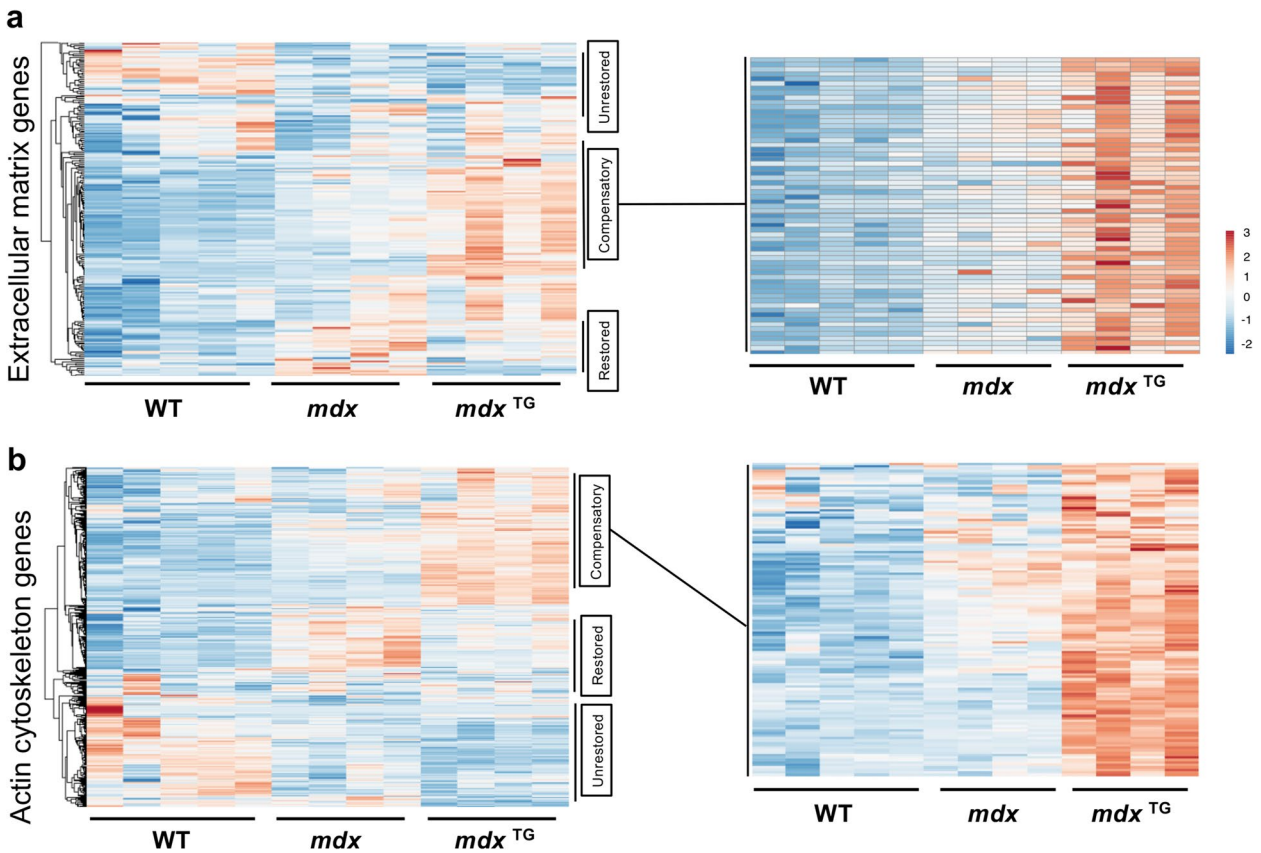

Fig. 2 SSPN overexpression results in compensatory upregulation of ECM and actin cytoskeleton genes. Heat maps of GO-term curated ECM genes (**a**) and actin cytoskeleton genes (**b**) from RNA sequencing data each with restored, unrestored, and compensatory expression patterns in the *mdx*^{TG} muscle. Expanded heat map insets emphasize that compensatory expression patterns are overwhelmingly from upregulated genes in the *mdx*^{TG} muscle

genes in the RNA sequencing data set based on GO categories and subsequently visualized this data using traditional heat maps. The actin cytoskeleton and ECM genes clustered into restored, unrestored, and compensatory categories. It is noteworthy that the compensatory genes represent the largest category of DEGs in this comparison (Fig. 2a–b, Supplementary Tables 2, 3).

We next analyzed the expression of ECM and cytoskeletal proteins from the mass spectrometry data set. ECM proteins were classified into 8 functional categories, including (1) structural ECM, (2) other ECM, (3) network collagen, (4) matricellular, (5) fibrillar collagen, (6) fibril-associated collagens with interrupted triple helices (FACIT), (7) ECM regulator, and (8) basement membrane proteins (Fig. 3a). Cytoskeletal proteins were classified into 9 functional categories, including (1) actins and microfilaments, (2) actin-associated, (3) tubulins, (4) microtubule associated, (5) annexins, (6) intermediate filaments, (7) spectrins, (8) myosins, and (9) sarcomere-associated proteins (Fig. 3b). ECM regulators and fibrillar collagens were upregulated in *mdx*^{TG} compared to both wild-type and *mdx* muscles (Fig. 3a). For cytoskeletal proteins, we observed significant downregulation in actins, microfilaments, and actin-associated proteins, as well as decreased abundance of myosins and other sarcomere-associated proteins such as tropomyosins and troponin I and T (Fig. 3b). Abundance of microtubule-associated proteins and spectrins was increased in *mdx*^{TG} samples relative to wild-type controls. Within each functional classification, we additionally identified several proteins with increased expression in *mdx*^{TG} muscle compared to both wild-type and *mdx* muscle including cathepsins and integrins (Fig. 4a), fibrillar collagens II, V, and XI (Fig. 4b), and non-erythrocyte β-spectrin (Sptbn1, spectrins, Fig. 4c). Interestingly, some actin isoforms and actin-associated proteins were decreased in *mdx*^{TG} muscle compared to both wild-type and *mdx* muscle including skeletal and cardiac α-actins (Acta1, Actc1) and α-actinin (Actn3, Fig. 4d).

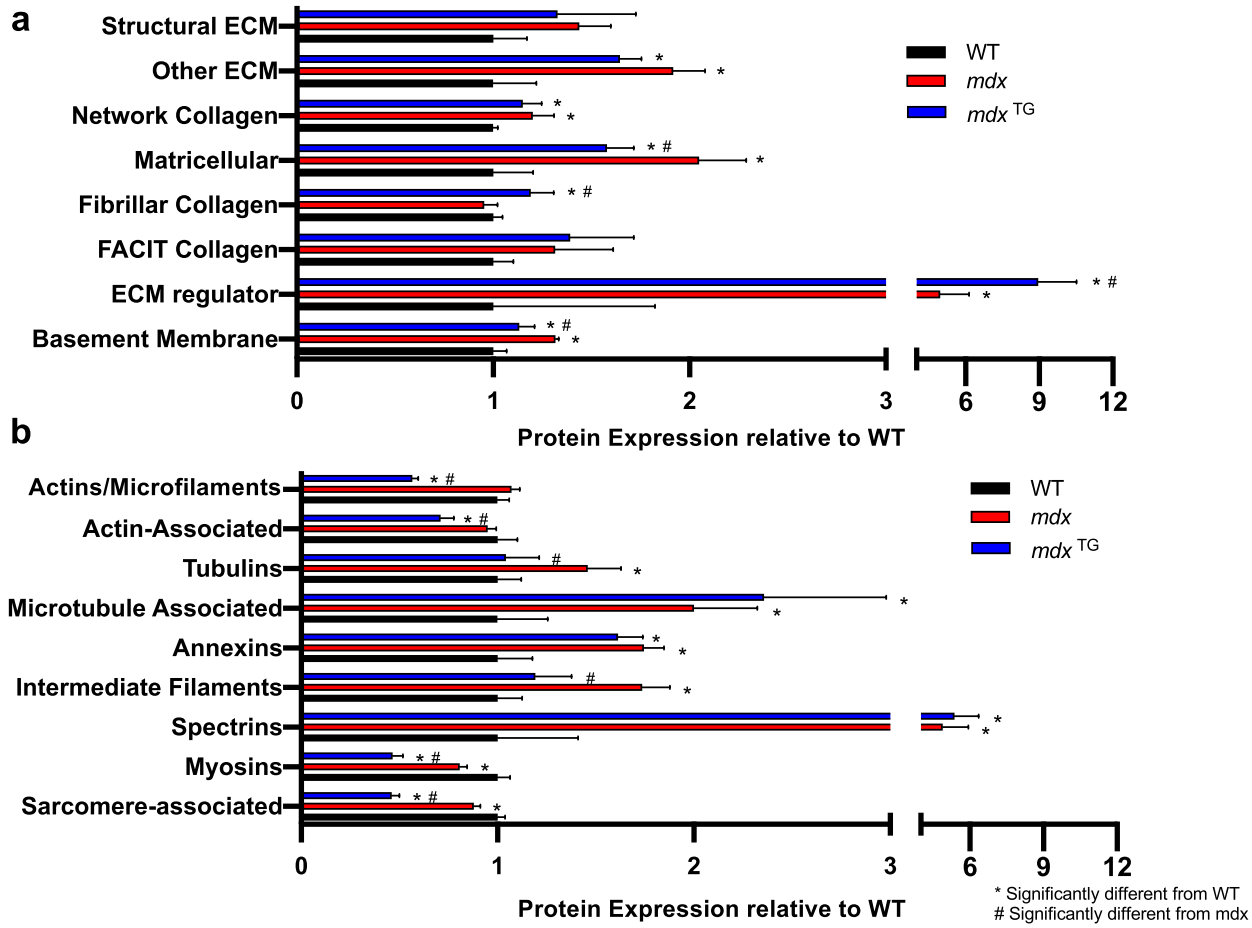

Fig. 3 Compensatory changes in functional classes of ECM and cytoskeletal proteins in mdx^{TG} muscle. **a** Graph of the abundance of ECM proteins in 8 primary categories relative to WT. **b** Graph of the abundance of cytoskeletal proteins in 9 primary categories relative to WT (*$p < 0.05$ compared to WT, #$p < 0.05$ compared to *mdx* by unpaired *t*-test. By category, mdx^{TG} muscle had compensatory expression (both significantly different from WT and *mdx*) of matricellular, ECM regulator, basement membrane, actins/microfilaments, actin-associated, myosins, and sarcomere-associated proteins

Proteomic analysis revealed compensatory upregulation of many collagens, including collagen type II (Col2) and collagen type V (Col5), along with upregulation of Sptbn1. Importantly, recent findings in the golden retriever model of DMD (GRMD) revealed spectrin as a candidate protein responsible for sparing of the cranial sartorius muscle from dystrophic pathology [54]. Spectrin is a mechanosensitive protein that functions as a scaffolding protein at the cell membrane to provide structural and mechanical stability [55]. Additionally, spectrin is a key linker protein in the response to mechanical stimuli, coupling changes in cellular tension to downstream signaling networks [56, 57]. The compensatory upregulation of spectrin along with fibrillar collagens suggests that SSPN overexpression may be rescuing the dystrophic phenotype through the alteration of mechanotransduction signaling networks.

Ingenuity pathway and gene set enrichment analyses support compensation through mechanotransduction pathways

To identify candidate networks and upstream regulators that drive compensatory changes in mdx^{TG} muscle, we analyzed the transcriptomic and proteomic data sets using the ingenuity pathway analysis (IPA) application. Based on the IPA upstream regulator algorithm and corresponding activation *z*-scores and *p*-values, we examined the top ten activated and inhibited upstream regulators for each comparison from the RNA sequencing (Fig. 5a) and mass spectrometry (Fig. 5b) data sets. Upon closer analysis of the top five activated and inhibited regulators, we observed many cytoskeletal and ECM target molecules (Table 1, Supplementary Tables 4–6, targets in bold red). Our analyses reveal that SSPN induces large-scale changes in the composition of the

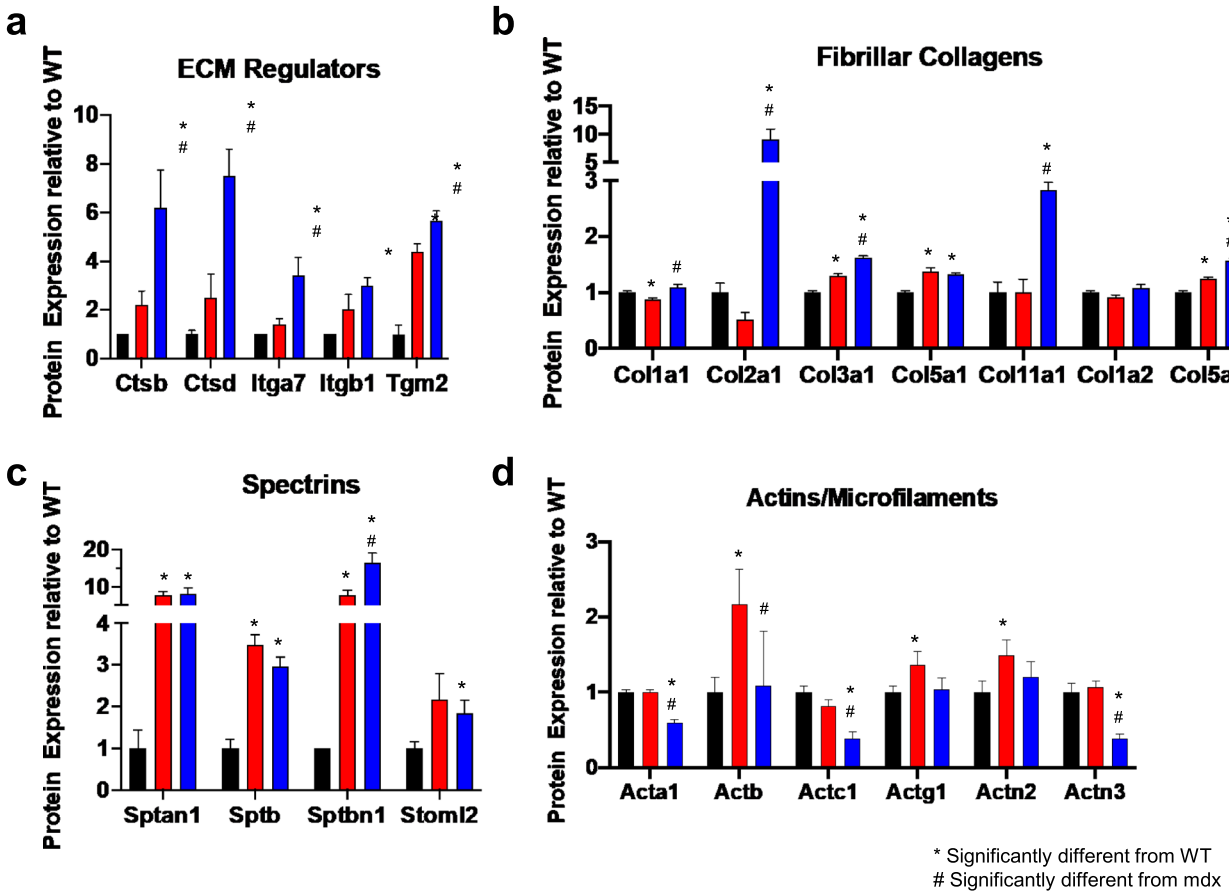

Fig. 4 Upregulation of ECM regulators, fibrillar collagens, and spectrins in mdx^{TG} muscle. Relative protein expression of ECM regulators (**a**), fibrillar collagens (**b**), spectrins (**c**), and actins/microfilaments (**d**) (*$p < 0.05$ compared to WT, #$p < 0.05$ compared to *mdx* by unpaired *t*-test)

ECM and cytoskeleton as well as their associated signaling networks. Thus, we sought to integrate data from the transcript and protein analysis to develop a more comprehensive model reflecting the overlap of signaling networks. We performed integrative gene set enrichment analysis on the significantly differentially expressed transcripts and proteins between *mdx* and mdx^{TG} (Fig. 6). This comprises the proteins and genes in the compensatory and restored categories. We observed enrichment of gene sets associated with signal transduction pathways affecting a broad spectrum of cellular and biological processes important in myogenesis, regeneration, and homeostasis of skeletal muscle involving the Ras, Rho, and Wnt signaling, actin-cytoskeleton remodeling and organization, and ECM signaling and organization (Fig. 6). These include signaling by Rho GTPases, regulation of cytoskeleton organization and cytoskeletal regulation by Rho GTPases, integrin signaling, focal adhesions formation, and response to mechanical stimulus (Fig. 6). We observed compensatory upregulation of Rho family of GTPases involved in mediating actin dynamics and actomyosin contractility including Ras homolog gene family members (RhoA and RhoC), Rac family small GTPase 1 (Rac1), and cell division cycle 42 (Cdc42). There are compensatory and restorative changes in several factors that regulate Rho GTPase activity including the GTPase activating proteins (Arhgap 6, 22, and 44), all of which are increased in mdx^{TG} muscle. Wnt proteins, including Wnt4 and Wnt5a, play key roles as part of the muscle regeneration program, cytoskeletal remodeling, and myoblast fusion [58, 59]. Wnt4 regulation of RhoA activity is important for maintaining satellite cell quiescence [59]. In addition, Wnt5a and Fzd4 (rescued in mdx^{TG}) have been shown to regulate osteogenic differentiation after mechanical stretch [60]. R-spondins family members 1 and 4 (Rspo1 and Rspo4) positively regulate the canonical Wnt signaling pathway and are important for muscle repair and regeneration [61–63]. RhoA and Rac1 can also be activated by and respond to mechanical stress and stimuli. At focal adhesion sites of integrin signaling, these proteins orchestrate actin cytoskeleton remodeling important for mechanical force generation

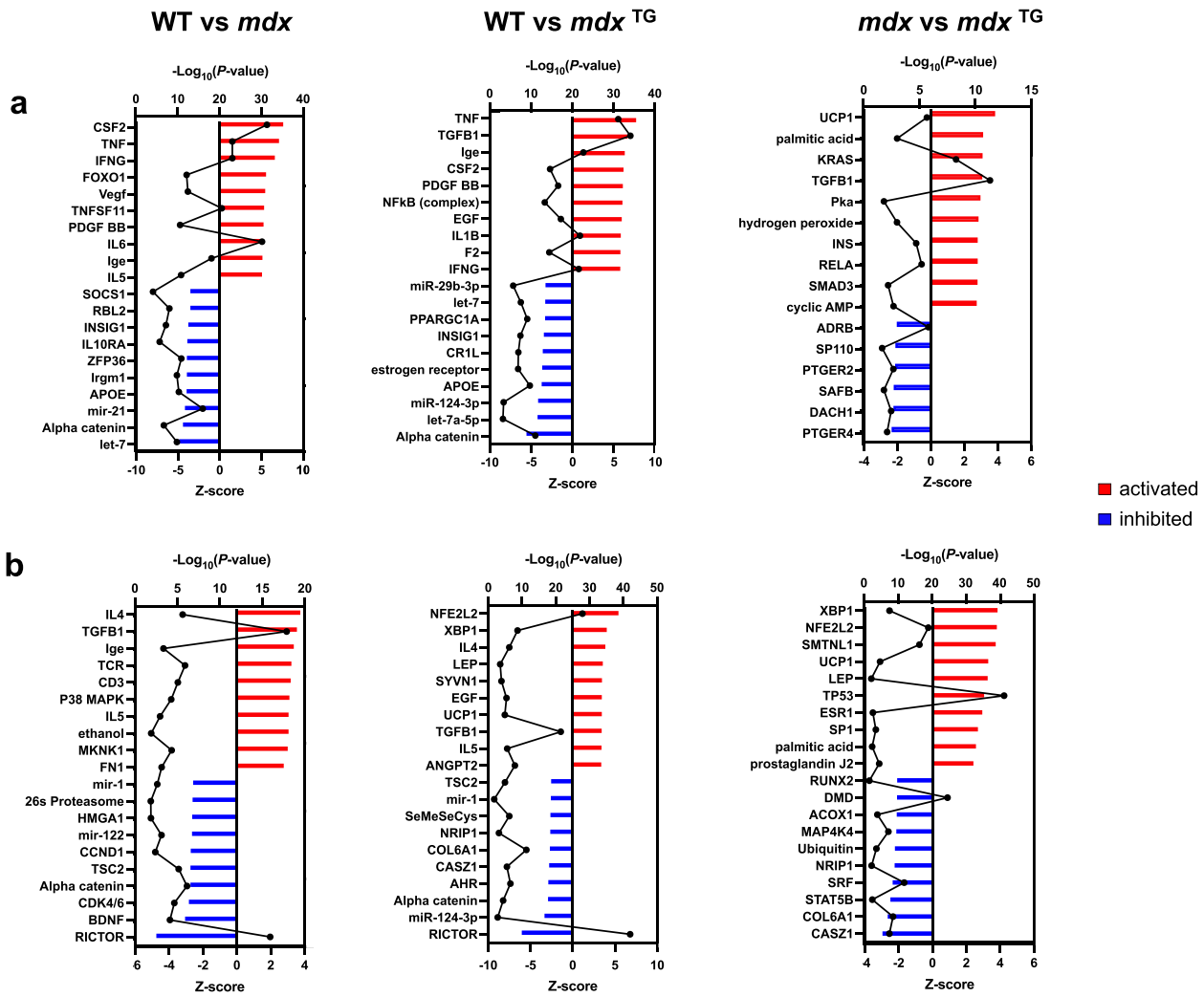

Fig. 5 Activated and inhibited upstream regulators identified in wild-type, *mdx* and *mdx*^{TG} muscle through ingenuity pathway analysis. Ingenuity pathway analysis (IPA) of RNA sequencing data (**a**) and mass spectrometry data (**b**) identifying the top 10 upstream regulators that are activated (*z*-score, red bars) or inhibited (*z*-score, blue bars) with −log *p*-values overlaid in black. Comparisons include WT vs *mdx* (left graphs), WT vs *mdx*^{TG} (middle graphs), and *mdx* vs *mdx*^{TG} (right graphs)

and transmission in concert with talin (Tln2) and vinculin (Vcl) [64]. Several integrin and laminin subunits are also alternatively expressed in *mdx*^{TG} relative to *mdx*. As we have shown previously, integrin alpha 7 (Itga7) is increased in *mdx*^{TG} muscle [27]. The cysteine and glycine-rich protein 3 (Csrp3, also known as muscle LIM protein, MLP) is localized at costameres and involved in promoting mechanical- and stress-induced myocyte differentiation and remodeling [65, 66]. Interestingly, transcription factors JunB and Sox9 are both upregulated in *mdx*^{TG} muscle. JunB is also important for maintaining muscle growth and hypertrophy [67]. Sox9, important for bone and cartilage formation, is expressed in muscle progenitor cells during development and may play a role in musculoskeletal development [68]. Sox9 has been shown to be a key regulator of ECM deposition, most specifically of collagen II [69], which is highly upregulated in *mdx*^{TG} muscle (Fig. 4).

To validate our findings from the mass spectrometry data and gene set enrichment analysis, we performed immunofluorescence analysis of muscle sections using antibodies against collagen II, collagen V, Sptbn1, yes-associated protein 1 (Yap1), and Sox9 (Fig. 7). Immunofluorescence analysis and quantification validate the mass spectrometry data showing increased collagens II and V and Sptbn1 in *mdx*^{TG} compared to WT and *mdx* muscle (Fig. 7a–b). The Hippo-Yap1 network also plays a significant role in the response to mechanical stimuli with potential implications in muscle development and homeostasis following Yap1 translocation

Table 1 Ingenuity pathway analysis summary — upstream regulators

Predicted Activation State	Upstream Regulator	Target molecules in dataset	Molecule Type	Activation z-score	p-value of overlap
WT vs *mdx* (Proteomics)					
Activated	Interleukin 4 (IL4)	ACOT9, **ACTG1**, ALDH2, **ANXA1**, **ANXA2**, **ANXA4**, APOE, **BIN1**, C3, **CAPG**, CCT3, Cdc42, CLTC, **COL18A1**, **COL1A1**, **COL6A2**, DYNC1H1, **FABP4**, **FN1**, GBE1, Hist1h1e, **LGALS1**, **LGALS3**, **MAP4**, **MYH9**, NCL, Nedd4, PLEC, **POSTN**, RPS6, **SPTBN1**, **TGFBI**, **TGM2**, TLN1, TLN2, **VARS**, **VIM**	cytokine	3.748	2.36E-06
	Transforming growth factor beta 1 (TGFB1)	>50 Target Molecules	growth factor	3.549	1.36E-18
	Immunoglobulin E (Ige)	**ANXA1**, C3, CAV1, **COL18A1**, **GSN**, NAPA, PFN1, PPIA(2), RAB7A, SERPINB1, SNRPD1, SNRPD3, **Tpm1**, **TUBB6**, **VIM**	complex	3.359	0.000421
	T-cell receceptor (TCR)	APOE, **BIN1**, ENO1, **HSPB1(1)**, HSPA5, **LMNB1**, P4HB, PGAM1, PHB2, RPL10A, RPL15, RPL22, RPL30, RPL4, RPLA, RPL7, RPLP0, RPS10, RPS3, **RPSA**, SNRPD3	complex	3.221	1.24E-06
	Cluster of differentiation 3 (CD3)	ACADS, **ACTR3**, **ANXA1**, CYC1, HNRNPA2B1, HPX, HSPB1, HSPA5, NCL, OGN, P4HB, PFN1, PGAM1, PHB2, PLEC, PPA1, PREP, PSAP, RPL30, RPLA, RPS14, S100A11, SLC25A5, STIM1, **SYNPO**, **TGM2**, VDAC2	complex	3.175	8.64E-06
	Rapamycin-insensitive companion to mTOR (RICTOR)	CTC1, NDUFB4, NDUFS1, NDUFV2, PPA1, PSMA6, PSMC2, PSMD2, RPL10, RPL10A, RPL11, RPL12, RPL14, RPL22, RPL23, RPL30, RPL4, RPL6, RPL7, RPL7A, RPLP0, RPS10, RPS18, RPS3, Rps3a1, RPS4Y1, RPS5, RPS6, RPS9, RPSA	other	-4.747	1.16E-16
Inhibited	Brain-derived neurotrophic factor (BDNF)	**ANXA2**, **ANXA5**, BAG3, GLUL, HSPA5, **LAMB2**, **LAMC1**, **LGALS1**, **MYH9**, **MYL6**, PREP, RNH1, RPL13, SERPINH1, **TUBA1A**, **VIM**	growth factor	-3.051	7.39E-05
	Cyclin-dependent kinase 4/6 (CDK4/6)	ENO1, HSPB1, **LAMB2**, RPL10, RPL13, RPL27A, RPS6, **TUBB**	group	-2.828	0.000022
	Alpha catenin	**BGN**, **COL1A1**, **COL3A1**, **COL5A1**, **COL5A2**, **COL6A1**, **COL6A2**, **LAMA2**, **LAMA4**, **LUM**, **TGM2**, **VIM**	actin assembly	-2.729	7.28E-07
	Tuberous Sclerosis Complex 2 (TSC2)	**ANXA1**, **ANXA2**, CRYAB, GSN, HSPA5, HSPB1, **LGALS3**, PVALB, Rpl32, S100A11, S100A6	other	-2.728	6.83E-06
WT vs *mdx* TG (Proteomics)					
Activated	Nuclear factor, erythroid 2-like 2 (NFE2L2)	ALDH3A, ARPC1, ATP1A2, Cdc42 (includes others), CAT, CBR1, CCT7, **COL18A1**, **CTSD**, DSTN, EIF3E, ESD, **FABP5**, **FN1**, FTH1, GBE1, GPX1, GSTM5, GSTO1, HSP90AA1, HSPB1(1), IDH1, **LMNA**, ME1, NARS, PCBP1, PDIA3, PDIA6, PGD, PHKA1, PPIB, PRDX1, PSMA1, PSMA4, PSMA5, PSMA6, PSMA7, PSMB2, PSMB4, PSMB5, PSMD13, PSMD2, PSMD7, **RAC1**, RAN, RARS, RPL18, RPL9, RPS16, S100A13, SEC23A, SERPINA3, TALDO1, **TPI1**, **Tuba1**, TTR, USO1, USP14, VCP	transcription factor	5.416	1.21E-28
	X-box binding protein (XBP1)	APOA1, ARCN1, ATP2A2, CALR, CAT, DDOST, ERP44, FN1, HSP90B1, HSPA5, PDIA3, PDIA6, PPIB, RPN1, RPN2, S100A6, SEC23A, SERPINA1, SSPB1, SUB1, TTR, USO1, WFS1	transcription regulator	4.027	1.98E-09
	Interleukin 4 (IL4)	ACOT9, ACOX1, ALDH2, **ANXA1**, **ANXA2**, **ANXA4**, ATP2A2, BIN1, C3, CAPG, CAT, **Cdc42**, **CLIP1**, CLTC, **COL18A1**, **COL6A2**, DECR1, DYNC1H1, EPHX1, **FABP4**, **FN1**, GBE1, GPT, GPX4, HUFD, HSPA1A/HSPA1B, **ITGB1**, **LGALS1**, MAP4, MARCO, MTDH, **MYH9**, NCL, Nedd4, PHB, **PLEC**, **POSTN**, PSMA6, **RHOA**, **SPTBN1**, **TGM2**, TINAGL1, TLN1, TLN2, TNC, UCHL3, USO1, VARS, **VIM**, VPS35	cytokine	3.867	5.92E-07
	Leptin (LEP)	ACADL, ACOX1, APOA1, APOB, ATP2A2, CAV1, **COL2A1**, **COL3A1**, **COL4A1**, ECH1, FABP4, FHP2, GAPDH, GOT2, GPX1, HPX, HSPA5, IDH1, NAMPT, OPLAH, PRDX1, **RAC1**, SLC25A5, **VIM**	growth factor	3.568	0.000295
	Synoviolin 1 (SYVN1)	ATP1A1, HNRNPM, HSPB1, **ITGB1**, LDHB, PCBP1, PFN1, RAB10, RPLS0, RPL18, RPN2, USP5	transporter	3.464	0.000125
Inhibited	Rapamycin-insensitive companion to mTOR (RICTOR)	Arp5c, ATP5F1C, ATP5H, H5G, COX5A, Cox5b, COX6B1, CYC1, NDUFA7, NDUFB10, NDUFB1, NDUFB7, NDUFB8, NDUFS1, Nduf5, NDUFS6, NDUFV1, PPA1, PSMA1, PSMA2, PSMA4, PSMA5, PSMA6, PSMA7, PSMB2, PSMB4, PSMB5, PSMB7, PSMC4, PSMD13, PSMD3, PSMD5, PSMD7, RPL10, RPL11, RPL12, RPL13A, RPL18, RPL23, Rpl23a, RPL26, RPL28, RPL30, Rpl34 (includes others), RPL35A, RPL4, RPL7, RPL8, RPLA, RPLP0, RPLP2, RPS11, RPS19, RPS21, RPS27A, RPS3, RPS4Y1, RPS5, RPS9, RPSA, SDHA, SDHB, UQCRH,	other	-6.016	8.73E-43
	miR-125-3p (and other miRNAs w/seed AAGGCAC)	ACAA2, CAV1, EC2, GBP1, GSN, HADH, HADHB, **ITGB1**, **LMNB1**, **MYH9**, PDLIM7, SUB34, TLN1, **TUBB6**	mature microRNA	-3.329	0.00152
	Alpha catenin	**COL15A1**, **COL3A1**, **COL5A1**, **COL5A2**, **COL6A1**, **COL6A2**, **CTSB**, KRT4B, **LAMA4**, **TGM2**, TNC, **VIM**	group	-2.911	3.69E-05
	Aryl hydrocarbon receptor (AHR)	ACOX1, ALDH2, ASPN, CBR1, **Cdc42**, **COL1A1**, **COL1A2**, **COL3A1**, **COL4A1**, **COL5A1**, **COL6A2**, **COL6A3**, **CTSD**, ENO1, FABP4, **FN1**, Gm21596/Hnrnpb1, GSTM5, HSPA9A/A1, HSPA5, **ITGA7**, LDHA, **MYL2**, **NID2**, SST-A1, **VCL**, **VIM**	ligand-dependent nuclear receptor	-2.874	2.65E-07
	Castor zinc finger (CASZ1)	**ACTA1**, CASQ1, CKM, **COL2A1**, **ITGA7**, **MYH3**, **MYOZ1**, **TNNI2**	enzyme	-2.778	2.99E-06
***mdx* vs *mdx* TG (Proteomics)**					
Activated	X-box binding protein 1 (XBP1)	APOA1, ATP2A2, CALR, CAT, DUP4L, HSP90B1, HSPA5, PDIA3, PDIA6, RPN1, RPN2, SEC23A, SERPINA1, SOD1, SSPB1, SUB1A, TTR, USO1, WFS1	transcription regulator	3.854	3.63E-08
	Nuclear factor, erythroid 2-like 2 (NFE2L2)	**ACTG1**, ALDH3A, ATP1A1, Cdc42 (includes others), CAT, CBR1, CCT7, **COL1A1**, **COL3A1**, **CTSD**, EIF3E, FABP5, FTH1, GBE1, GPX1, GSTM1, GSTO1, HSP90AA1, HSPB1(1), **LMNA**, ME1, PAFAH1B1, PCBP1, PDIA3, PDIA6, PGD, PHKA1, PREP, PSMA1, PSMA5, PSMA6, PSMA7, PSMB4, PSMB5, PSMD13, SEC23A, SERPINA3, SOD1, TALDO1, **TPI1**, **Tpm1**, TTR, TXNRD1, USO1	transcription regulator	3.805	1.45E-08
	Smoothelin-like protein 1 (SMTNL1)	**ACTA1**, Cdh1, FLNC, GAPDH, **MYH1**, **MYL1**, **MYOM1**, PFKM, PYGM, **TNNC2**, **TNNI2**, **TNNT3**, **Tpm1**, **Tpm2**	other	3.742	5.89E-17
	Uncoupling protein 1 (UCP1)	ACOT2, BCAT2, GARS, GPX3, GPX4, GSTM1, GSTO1, MTHFD1, **MYH4**, NDUFS3, PGD, SDHB, SYNM	transporter	3.302	0.000022
	Leptin (LEP)	ACADVL, APOA1, APOE, ATP2A2, **COL1A1**, **COL2A1**, **COL3A1**, **COL4A1**, ECH1, ETFDH, FABP4, GAPDH, HSPA5, NAMPT, OPLAH, **RAC1**, SOD1	growth factor	3.269	0.00776
Inhibited	Castor zinc finger 1 (CASZ1)	**ACTA1**, CASQ1, CKM, **COL2A1**, **ITGA7**, MYOZ1, MYPN, **NEFL**, **TNNI2**	enzyme	-2.95	3.85E-08
	Collagen type VI alpha 1 chain (COL6A1)	AK1, ALDOA, CKM, ENO3, PVALB, **TNNI2**, TPI1	other	-2.646	3.21E-09
	Signal transducer and activator of transcription 5B (STAT5B)	**ACTC1**, ATP2A2, CBR1, MDH2, ME1, **MYH7**, **MYL1**, **MYL2**, **MYL4**, RPLS, **TNNC1**, **TNNI1**, **TPM3**	transcription regulator	-2.481	0.0043
	Serum response factor (SRF)	**ACTA1**, **ACTB**, **ACTC1**, **ACTG1**, CKM, CPA3, **DES**, FHL1, HSPA2, **LDB3**, LMCD1, **MYH4**, **MYH7**, **MYL1**, **MYL2**, **MYL3**, **MYL4**, **MYLPF**, **MYOM1**, PAFAH1B1, PDLIM7, RNH1, **SMTN**, SVIL, TAGLN, **TNNC1**, **Tpm1**, **Tpm2**, TTN, **TUBB4B**, **VCL**	transcription regulator	-2.353	1.7E-12
	Nuclear receptor interacting protein 1 (NRIP1)	ACAA2, APOA1, LDHB, OPLAH, SDHB	transcription regulator	-2.236	0.00682

to the nucleus [57, 70]. To gain further insight on this downstream mechanotransduction signaling pathway, we quantified the percentage of nuclear Yap1 translocation following indirect immunofluorescence and found an increase in *mdx*^{TG} muscle relative to WT and *mdx* muscle (Fig. 7c, Supplemental Fig. 3). Interestingly, our results also indicated profound sarcolemmal localization of Yap1 in *mdx*^{TG} muscle. Furthermore, immunofluorescence analysis of muscle sections reveals increased Sox9 protein in *mdx*^{TG} muscle, and that in addition to nuclear localization, Sox9 is abundant at the sarcolemma and neuromuscular junction where it co-localizes with α-bungarotoxin (Fig. 7c). While Yap1 and Sox9 typically localize to the cytoplasm and/or nucleus, previous reports have also described sarcolemmal and connective tissue localization in muscle [70–72]. Overall, our analyses indicated that SSPN overexpression in dystrophin-deficiency results in a rewiring of signaling networks associated with cell-matrix communication and mechanotransduction.

To visualize the differential expression pattern of the key components of the ECM and cortical cytoskeleton, we prepared a schematic from both transcriptomic and proteomic perspectives using a color key (Fig. 8). As shown in the summary figure, the differential expression pattern of many of the key players of mechanotransduction at the cell-matrix interface reveals the compensatory effects of SSPN overexpression.

Discussion

In our multi-omics approach to identifying mechanisms of SSPN amelioration of dystrophic pathology, we built on previous comparative transcriptomic and proteomic studies that have identified the molecular changes in *mdx* muscle throughout progression of disease in muscle groups that are differentially affected by disease [37, 40, 42, 73]. Our approach combines RNA sequencing transcriptomics with ECM-optimized capture techniques to identify SSPN-induced cellular pathways. Findings from our proteomic analysis reveal compensatory alterations in the abundance of collagens in *mdx*^{TG} muscle, especially the highly glycosylated collagens II, V, and XI. Collagen is the most abundant protein in the ECM, and its high tensile strength allows transmission of forces generated by skeletal muscle fibers. The most abundant collagens in skeletal muscle are collagens I, III, IV, and VI. While collagens were upregulated in the *mdx*^{TG}, they were primarily collagens not typically observed in skeletal muscle, or those of low abundance, including collagens II, V, and XI [74]. Collagen II is typically found in articular cartilage and intervertebral discs and is highly glycosylated [75, 76]. Collagen XI is also a component of cartilage extracellular matrix [77]. The presence of these bulky

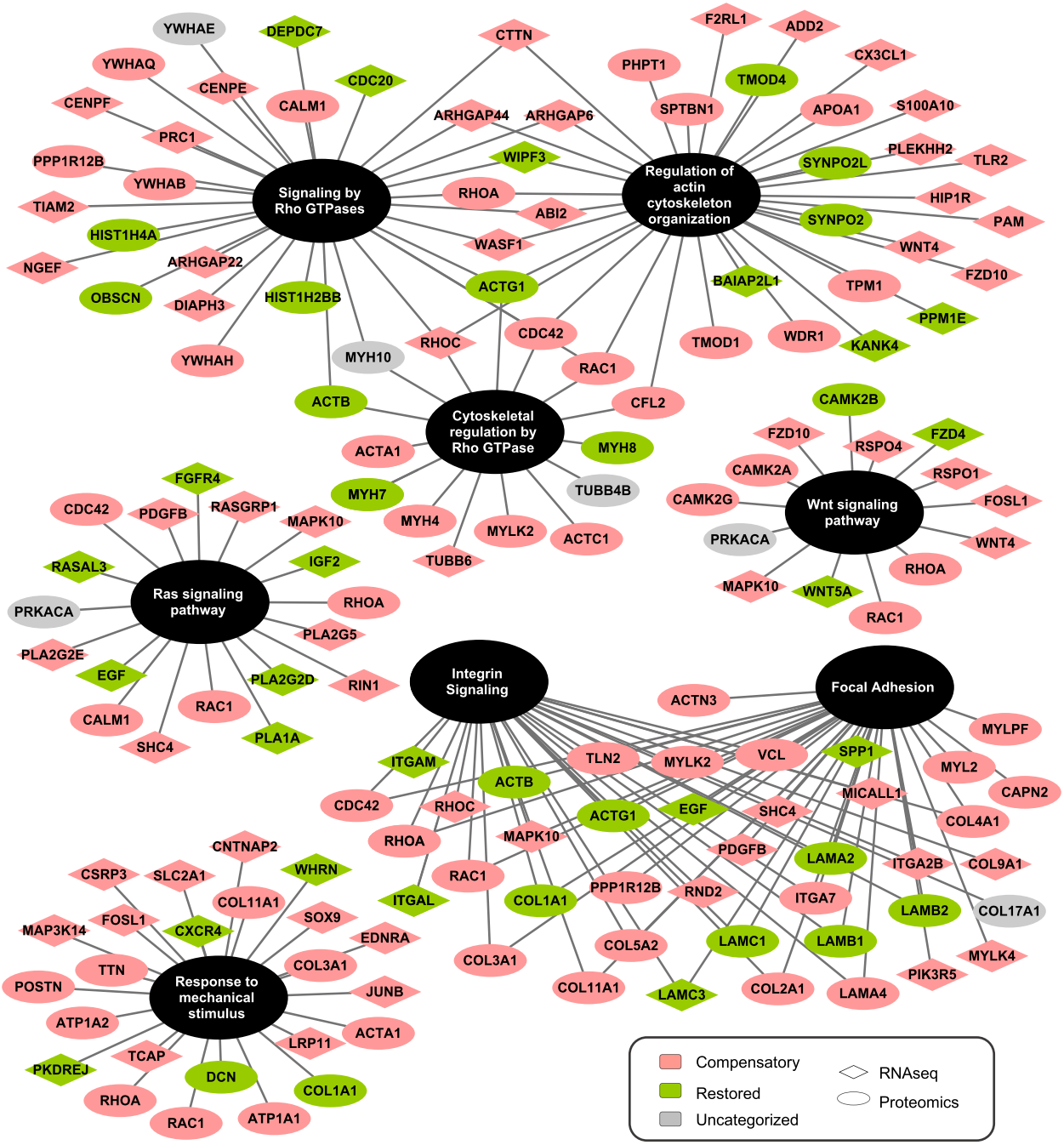

Fig. 6 Integrated gene set enrichment analysis identifies differential expression of mechanosignaling pathways in *mdx*^{TG}. To develop an integrated model of overlapping signaling networks driving rescue of the *mdx*^{TG} skeletal muscle, we combined transcripts (diamonds) and proteins (ovals) that were differentially expressed between *mdx* and *mdx*^{TG} tissue and performed gene set enrichment analysis. Compensatory changes are in pink, restored changes are in green, and uncategorized changes are in gray. The gene set enrichment analysis highlights changes in Rho, Rac, Wnt, and integrin signaling in addition to cell adhesion and response to mechanical stimulus

disaccharide groups is believed to hinder the formation of highly ordered fibrils and has been shown to increase substrate compliance in co-cultures with collagen I [78]. Collagens V and XI are typically observed only during skeletal muscle development; however, the function of collagen XI in skeletal muscle is unknown. Baghdadi and colleagues [79] recently reported that satellite cells produce collagen V that is critical for the calcitonin receptor and notch signaling cascade, which maintains satellite cells in a quiescent state. Taken together, the changes

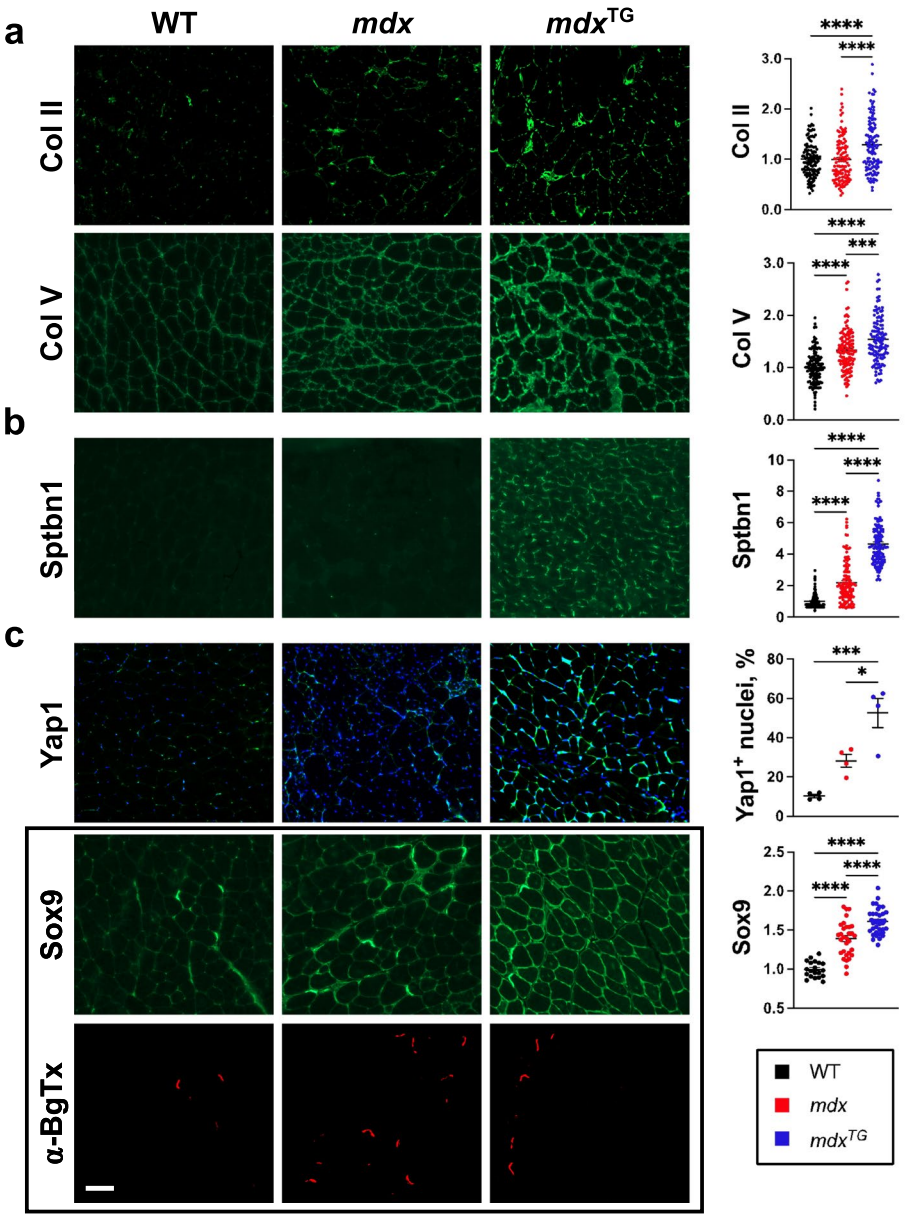

Fig. 7 Validation of signaling and mechanosensitive pathways increased in *mdx*^{TG} muscle. Indirect immunofluorescence analysis and quantification of 12-week-old mouse quadriceps using antibodies against (**a)** collagen II (Col II) and collagen V (Col V), (**b)**β-spectrin (Sptbn1), (**c)** yes-associated protein 1 (Yap1) and SRY-Box transcription factor 9 (Sox9) showing increased abundance in *mdx*^{TG} relative to both WT and *mdx*. Sox9 is expressed at the neuromuscular junction shown by co-localization with α-bungarotoxin (α-BgTx). Statistical analyses were performed by one-way ANOVA with Tukey's multiple comparison tests, $n = 3$–4 biological replicates per genotype, data represented as +/− SEM (*$p < 0.05$, **$p < 0.01$, ***$p < 0.001$, ****$p < 0.0001$). Scale bar = 100 µm

observed in the *mdx*^{TG} ECM suggest that upregulation of these developmental and cartilaginous collagens may be beneficial to muscle.

The identification of β-spectrin upregulation as another potential compensatory protein is supported by data from the GRMD dog model of DMD. Nghiem and colleagues [54] identified spectrin as a candidate protein in a study of the cranial sartorius muscle that is spared from dystrophic pathology through compensatory hypertrophy via myostatin signaling. Spectrin is a scaffolding protein that functions to localize and stabilize surface proteins in nonerythroid cells, anchoring them to the cytoskeletal actin network [80]. The repeated triple helical units of the spectrin rod domain would support this function by stabilizing surface proteins and mediating cell-matrix and cell-cell

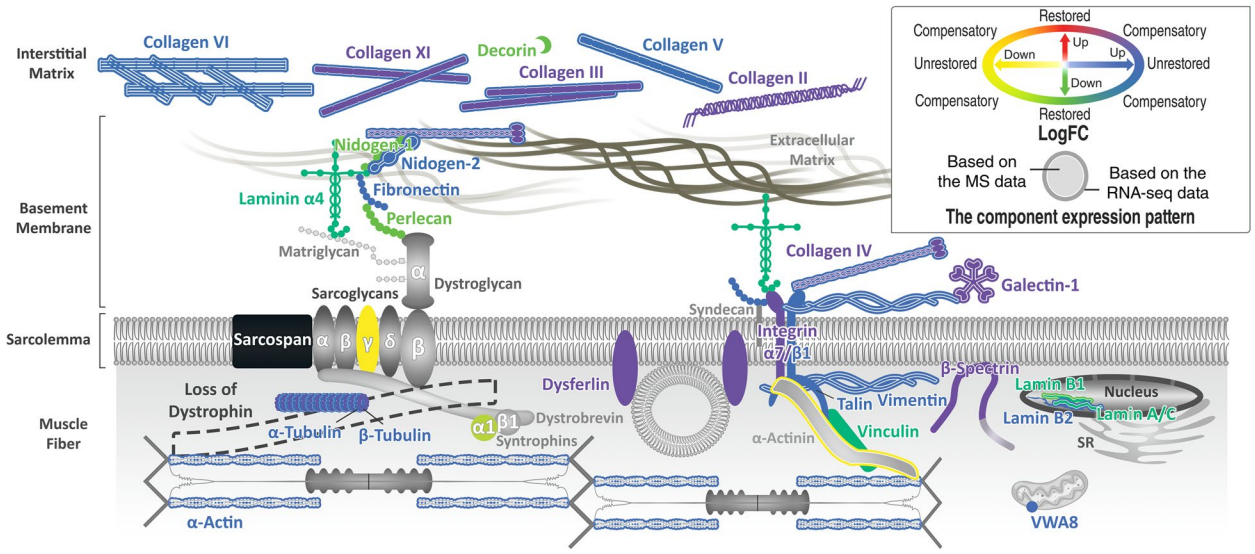

Fig. 8 SSPN overexpression rewires ECM-cell communication. Schematic summarizing ECM and cytoskeletal changes in RNA sequencing and proteomic data sets. Changes in gene or protein expression are represented by color according to the key, indicating compensatory upregulation of many ECM and cytoskeletal molecules with downstream signaling effects (in purple). The *x*- and *y*-axes in the color key correspond to *mdx*^{TG} relative to WT and *mdx*^{TG} relative to *mdx*, respectively

interactions. Interestingly, dystrophin contains similar spectrin-like repeats in its central rod domain and has been reported to bind spectrin [81–83]. Data from the IPA and gene enrichment analysis also identify spectrin as a target molecule of signaling pathways associated with a reorganization of the actin cytoskeleton. Together, the upregulation of collagens and scaffolding cytoskeletal components such as spectrin suggests that SSPN overexpression and the increase of adhesion complexes at the membrane may induce a rewiring of signaling between the ECM and the cytoskeleton to stabilize the sarcolemma during contraction and enhance mechanotransduction in order to improve force transmission.

Mechanotransduction has been described in the *mdx* mouse model in many studies that highlight the role of microtubules, adhesion complexes, mechanosensitive ion channels, and YAP/TAZ signaling in both skeletal and cardiac muscle pathology [70, 84–89]. Our study corroborates some of these findings at the transcript level when comparing wild-type and *mdx* muscle (Supplementary Fig. 2). At the protein level, we observed increased Yap1 localization in the nucleus of *mdx*^{TG} muscle (Fig. 7). Spectrin has also been shown to be a linker protein that couples mechanical stimuli to downstream signaling networks, including Hippo-YAP/TAZ pathway [56, 57]. Together, these data suggest that SSPN is improving force transmission in part through spectrin-Yap1 mechanotransduction pathways. Our gene set enrichment analysis revealed potential candidate alternative pathways involved in mechanotransduction through regulation of cytoskeleton, focal adhesion, and integrin signaling (Fig. 6). Notably, we identified compensatory changes in RhoA, Rac, and Wnt signaling molecules in the *mdx*^{TG} muscle. Reciprocal cross talk between the Wnt, Rho GTPase, and the integrin complex mediates cell adhesion signaling cascades and regulation of the cytoskeleton [90–92]. Integrins are bidirectional mechano-transducers that detect mechanical cues and translate these signals to affect intracellular and extracellular behavior and response. Through its interaction with adaptor proteins at sites of focal adhesion, the integrin complex regulates the dynamic, cyclic, spatial, and temporal activation of RhoA, Rac1, or Cdc42 leading to actin polymerization and depolymerization which drives force propagation, cell motility, and contractility [90, 93, 94]. RhoA, through downstream effectors, stabilizes actin filaments and regulates the activity of cofilin 2 (CFL2) which together with WD repeat-containing protein 1 (Wdr1) engages in depolymerization and severing of actin filaments, important to replenishing the actin monomer pool, while Rac1 and cdc42 are involved with activation of Wiskott-Aldrich syndrome protein family member 1 (Wasf1) and Abl interactor 2 (ABI2), members of the WAVE complex, to promote actin nucleation and branching [95]. Obscurin (Obscn), a sarcomeric rho-guanine nucleotide exchange factor [96], has been shown to activate RhoA in skeletal muscle [97].

Adducin 2 (Add 2) functions to cap the barbed end of actin filaments and is involved with recruiting spectrin tetramers to actin filaments [98, 99]. Rac1 and cdc42 have also been reported to signal through the DGC complex and may be downregulated during muscle atrophy [100]. Furthermore, RhoA, in addition to Rac1 and Cdc42, regulate transcription by SRF [101]. Interestingly, the transcription factor SRF is in one of the top five significantly inhibited/affected upstream regulators in our IPA analysis between *mdx* and *mdx*^{TG} (Table 1). Additionally, we identified compensatory changes in Sox9 in *mdx*^{TG} muscle with the gene set enrichment analysis, and we validated this at the protein level. Sox9 has been identified as a key transcription factor involved in ECM deposition in cartilage tissue, specifically collagen II [69]. Our findings of compensatory changes in muscle of other cartilage-related proteins including collagen II and collagen XI are novel and suggest a possible new mechanism of improved force transmission in dystrophic muscle.

Conclusions

We generated a data-driven schematic of the *mdx* muscle rescued by SSPN overexpression that highlights compensatory changes in the ECM and cytoskeleton at both the transcript and protein level (Fig. 8). Our multi-omics data suggest that SSPN rescues dystrophin deficiency partially through a rewiring of cell-matrix interactions that may enhance mechanotransduction signaling cascades and improve lateral force transmission.

Abbreviations

DGC	Dystrophin-glycoprotein complex
ECM	Extracellular matrix
SSPN	Sarcospan
DMD	Duchenne muscular dystrophy
SG	Sarcoglycans
hSSPN	Human sarcospan
mSSPN	Mouse sarcospan
CPM	Counts per million
DEG	Differentially expressed genes
BSA	Bovine serum albumin
PBS	Phosphate-buffered saline
GO	Gene ontology
GRMD	Golden retriever model of DMD
IPA	Ingenuity pathway analysis
ESR1	Estrogen receptor 1
Col2/Col II	Collagen type II
Col5/Col V	Collagen type V
Sptbn1	Non-erythrocyte β-spectrin
Rac1	Rac family small GTPase 1
Cdc42	Cell division cycle 42
Arhgap	GTPase-activating proteins
TLN2	Talin
VCL	Vinculin
Itga7	Integrin alpha 7
Wasf1	Wiskott-Aldrich syndrome protein family member 1
ABI2	Abl interactor 2
Obscn	Obscurin
Add 2	Adducin 2
CFL2	Cofilin 2
Wdr1	WD repeat-containing protein 1
Csrp3	Cysteine and glycine-rich protein 3
Sox9	SRY-box transcription factor 9
JunB	JunB proto-oncogene, AP-1 transcription factor subunit
Yap1	Yes-associated protein 1
TAZ	Transcriptional coactivator with PDZ-binding motif
Col2a1	Collagen type II alpha 1 chain
Rho	Ras homolog
RAC	Rac family small GTPase
Wnt4	Wingless-type MMTV integration site family, member 4
Wnt5	Wingless-type MMTV integration site family, member 5
NAD/NADP	Nicotinamide adenine dinucleotide/nicotinamide adenine dinucleotide phosphate
GTPases	Guanosine triphosphate hydrolases
Ras	Rat sarcoma virus family protein
RhoA	Ras homolog family member A
RhoC	Ras homolog family member C
Fzd4	Frizzled class receptor 4
Rspo1	R-spondin 1
Rspo4	R-spondin 4
cdc42	Cell division cycle 42
WAVE complex	WASP-family verprolin homolog complex

Supplementary Information

The online version contains supplementary material available at https://doi.org/10.1186/s13395-022-00311-x.

Additional file 1: Supplementary Figure 1. Enrichment analysis was performed using the Database for Annotation, Visualization and Integrated Discovery platform (DAVID, version 2021) and identified Gene ontology terms, denoted as nodes for both the RNA sequencing (right half of nodes) and mass spectrometry (MS) datasets (left half of nodes). **Supplementary Figure 2.** Gene expression from RNA sequencing of genes associated with YAP/TAZ signaling (a) or Wnt signaling (b) in WT, *mdx*, and *mdx*^{TG} muscle in counts per million (CPM). **Supplementary Figure 3.** Additional images of indirect immunofluorescence analysis of 12-wk-old mouse quadriceps using an antibody against yes-associated protein 1 (Yap1) showing increased Yap1 signal in *mdx* and *mdx*^{TG} tissue showing possible immune cell Yap1 staining in *mdx* tissue. **Supplementary Table 1.** Summary of SSPN-Tg murine lines. **Supplementary Table 2**. RNA_ECM. **Supplementary Table 3.** RNA_Actin Cytoskeleton. **Supplementary Table 4.** Ingenuity Pathway Analysis – RNAsequencing WT vs *mdx*. **Supplementary Table 5.** Ingenuity Pathway Analysis – RNAsequencing WT vs *mdx*^{TG}. **Supplementary Table 6.** Ingenuity Pathway Analysis – RNAsequencing *mdx* vs *mdx*^{TG}.

Acknowledgements

We thank Dr. Ekaterina Mokhonova (UCLA) and Katherine Hammond for providing all tissues and mouse colony oversight, genotyping, and maintenance. This work was supported by the QCB Collaboratory community directed by Dr. Matteo Pellegrini (UCLA).

Authors' contributions

CS, EG, JLM, KSR, HM, and RHC conceptualized the project, study design, and methodology. RHC oversaw and coordinated the project. YZK performed initial computational analysis of the RNA sequencing data, and JLM, HM, CS, EG, and KSR further developed the analysis, visualization, and interpretation of the results. PK performed immunofluorescence analysis and quantification. KH and LRS performed the mass spectrometry with initial analysis, and KSR, JLM, EG, and HM further developed analysis and interpreted the results. CS, JLM, KSR, and EG analyzed and interpreted the ingenuity pathway analysis. MHA conceptualized and performed the gene ontology enrichment analysis and data visualization. KMS validated key findings using immunofluorescence

microscopy. HM proposed the rewiring concept and performed the integrative gene set enrichment to develop the model. JLM, KSR, and HM drafted the main manuscript, and JLM, KSR, HM, CS, PK, EG, and MHA prepared the figures in consultation with RHC. The authors read and approved the final manuscript.

Funding
This work was supported by funding from the National Institutes of Health (J. L. M.: IRACDA Fellowship K12 GM106996 and T32 AR065972; K. S. R.: T32 AR065972 and P50 AR052646; P. K.: T32 AR065972; E. M. G.: T32 AR059033 and F32 AR069469; C. S.: T32 AR065972; K. H.: R01 CA046934; R. H. C.: R01 AR048179, R01 HL126204), Muscular Dystrophy Association, USA (R. H. C.: 274143), and the UCLA Clinical and Translational Science Institute (K. S. R. and R. H. C.: UL1TR000124). Y. Z. K. was supported through a Quantitative and Computational Biology Collaboratory Postdoctoral Fellowship (UCLA). The funders had no role in the design of the study, data collection, analysis, interpretation of data, or in writing the manuscript.

Availability of data and materials
The proteomics dataset supporting the conclusions in this article is available in the PRIDE Archive repository. The RNA sequencing dataset supporting the conclusions in this article will be available on the NCBI GEO database upon publication.

Declarations

Ethics approval and consent to participate
Not applicable.

Consent for publication
Not applicable.

Competing interests
The authors declare that they have no competing interests.

Author details
[1]Department of Integrative Biology and Physiology, University of California, Los Angeles, CA 90095, USA. [2]Department of Orthopedic Surgery, David Geffen School of Medicine, University of California, Los Angeles, CA, USA. [3]Department of Biological Chemistry, Howard Hughes Medical Institute, David Geffen School of Medicine, University of California, Los Angeles, CA, USA. [4]Department of Biochemistry and Molecular Genetics, University of Colorado, Denver, CO, USA. [5]Department of Neurology, David Geffen School of Medicine, University of California, Los Angeles, CA, USA. [6]Molecular Biology Institute, University of California, Los Angeles, CA, USA. [7]Broad Stem Cell Research Center, University of California, Los Angeles, CA, USA.

Received: 9 July 2022 Accepted: 6 December 2022
Published online: 06 January 2023

References

1. Koenig M, Hoffman EP, Bertelson CJ, Monaco AP, Feener C, Kunkel LM. Complete cloning of the Duchenne muscular dystrophy (DMD) cDNA and preliminary genomic organization of the DMD gene in normal and affected individuals. Cell. 1987;50(3):509–17.
2. Hoffman EP, Brown RH, Kunkel LM. Dystrophin : the protein product of the Duchenne muscular dystrophy locus. Cell. 1987;51:919–28.
3. Rybakova IN, Patel JR, Ervasti JM. The dystrophin complex forms a mechanically strong link between the sarcolemma and costameric actin. J Cell Biol. 2000;150(5):1209–14 Available from: http://www.jcb.org/cgi/doi/10.1083/jcb.150.5.1209.
4. Ohlendieck K, Campbell KP. Dystrophin-associated proteins are greatly reduced in skeletal muscle from mdx mice. J Cell Biol. 1991;115(6):1685–94.
5. Ervasti JM, Campbell KP. Membrane organization of the dystrophin-glycoprotein complex. Cell. 1991;66(6):1121–31.
6. Cohn RD, Campbell KP. Molecular basis of muscular dystrophies. Muscle Nerve. 2000;23(10):1456–71 Available from: http://www.ncbi.nlm.nih.gov/pubmed/11003781.
7. Petrof BJ, Shrager JB, Stedman HH, Kelly AM, Sweeney HL. Dystrophin protects the sarcolemma from stresses developed during muscle contraction. Proc Natl Acad Sci U S A. 1993;90(8):3710–4.
8. Dumont NA, Wang YX, von Maltzahn J, Pasut A, Bentzinger CF, Brun CE, et al. Dystrophin expression in muscle stem cells regulates their polarity and asymmetric division. Nat Med. 2015;21(12):1455–63.
9. Dennett X, Shield LK, Clingan LJ, Woolley DA. Becker and Duchenne muscular dystrophy: a comparative morphological study. Aust Paediatr J. 1988;24(Suppl 1):15–20.
10. Kohler M, Clarenbach CF, Bahler C, Brack T, Russi EW, Bloch KE. Disability and survival in Duchenne muscular dystrophy. J Neurol Neurosurg Psychiatry. 2009;80(3):320–5.
11. Muntoni F, Mateddu A, Marchei F, Clerk A, Serra G. Muscular weakness in the mdx mouse. J Neurol Sci. 1993;120(1):71–7.
12. Briguet A, Courdier-Fruh I, Foster M, Meier T, Magyar JP. Histological parameters for the quantitative assessment of muscular dystrophy in the mdx-mouse. Neuromuscul Disord. 2004;14(10):675–82 [cited 2017 Mar 31]. Available from: http://www.ncbi.nlm.nih.gov/pubmed/15351425.
13. Connolly AM, Keeling RM, Mehta S, Pestronk A, Sanes JR. Three mouse models of muscular dystrophy: the natural history of strength and fatigue in dystrophin-, dystrophin/utrophin-, and laminin alpha2-deficient mice. Neuromuscul Disord. 2001;11(8):703–12.
14. Tinsley J, Deconinck N, Fisher R, Kahn D, Phelps S, Gillis J-M, et al. Expression of full-length utrophin prevents muscular dystrophy in mdx mice. Nat Med. 1998;4(12):1441–4 [cited 2018 Oct 10]. Available from: http://www.ncbi.nlm.nih.gov/pubmed/9846586.
15. Lamar K-M, Bogdanovich S, Gardner BB, Gao QQ, Miller T, Earley JU, et al. Overexpression of latent TGFβ binding protein 4 in muscle ameliorates muscular dystrophy through myostatin and TGFβ. PLoS Genet. 2016;12(5):e1006019.
16. Tjondrokoesoemo A, Schips T, Kanisicak O, Sargent MA, Molkentin JD. Genetic overexpression of Serpina3n attenuates muscular dystrophy in mice. Hum Mol Genet. 2016;25(6):1192–202.
17. Heller KN, Montgomery CL, Shontz KM, Clark KR, Mendell JR, Rodino-Klapac LR. Human alpha7 integrin gene (ITGA7) delivered by adeno-associated virus extends survival of severely affected dystrophin/utrophin-deficient mice. Hum Gene Ther. 2015;26(10):647–56.
18. Mázala DAG, Pratt SJP, Chen D, Molkentin JD, Lovering RM, Chin ER. SERCA1 overexpression minimizes skeletal muscle damage in dystrophic mouse models. Am J Phys Cell Phys. 2015;308(9):C699–709.
19. Baltgalvis KA, Jaeger MA, Fitzsimons DP, Thayer SA, Lowe DA, Ervasti JM. Transgenic overexpression of γ-cytoplasmic actin protects against eccentric contraction-induced force loss in mdx mice. Skelet Muscle. 2011;1(1):32 [cited 2013 Jan 22]. Available from: http://www.pubmedcentral.nih.gov/articlerender.fcgi?artid=3214766&tool=pmcentrez&rendertype=abstract.
20. Martin PT, Xu R, Rodino-Klapac LR, Oglesbay E, Camboni M, Montgomery CL, et al. Overexpression of Galgt2 in skeletal muscle prevents injury resulting from eccentric contractions in both mdx and wild-type mice. Am J Phys Cell Phys. 2009;296(3):C476–88.
21. Handschin C, Kobayashi YM, Chin S, Seale P, Campbell KP, Spiegelman BM. PGC-1alpha regulates the neuromuscular junction program and ameliorates Duchenne muscular dystrophy. Genes Dev. 2007;21(7):770–83.
22. Smith TC, Vasilakos G, Shaffer SA, Puglise JM, Chou CH, Barton ER, et al. Novel γ-sarcoglycan interactors in murine muscle membranes. Skelet Muscle. 2022;12(1) [cited 2022 Jun 16]. Available from: https://pubmed.ncbi.nlm.nih.gov/35065666/.
23. Dowling P, Gargan S, Murphy S, Zweyer M, Sabir H, Swandulla D, et al. The dystrophin node as integrator of cytoskeletal organization, lateral force transmission, fiber stability and cellular signaling in skeletal muscle. Proteomes. 2021;9(1):1–20 [cited 2022 Jun 16]. Available from: https://pubmed.ncbi.nlm.nih.gov/33540575/.
24. Crosbie RH, Heighway J, Venzke DP, Lee JC, Campbell KP. Sarcospan, the 25-kDa transmembrane component of the dystrophin- glycoprotein complex. J Biol Chem. 1997;272(50):31221–4.
25. Crosbie RH, Lebakken CS, Holt KH, Venzke DP, Straub V, Lee JC, et al. Membrane targeting and stabilization of sarcospan is mediated by the sarcoglycan subcomplex. J Cell Biol. 1999;145(1):153–65.
26. Crosbie RH, Lim LE, Moore SA, Hirano M, Hays AP, Maybaum SW, et al. Molecular and genetic characterization of sarcospan:

insights into sarcoglycan-sarcospan interactions. Hum Mol Genet. 2000;9(13):2019–27.
27. Peter AK, Marshall JL, Crosbie RH. Sarcospan reduces dystrophic pathology: stabilization of the utrophin-glycoprotein complex. J Cell Biol. 2008;183(3):419–27 [cited 2019 Nov 23]. Available from: http://www.ncbi.nlm.nih.gov/pubmed/18981229.
28. Marshall JL, Oh J, Chou E, Lee JA, Holmberg J, Burkin DJ, et al. Sarcospan integration into laminin-binding adhesion complexes that ameliorate muscular dystrophy requires utrophin and α7 integrin. Hum Mol Genet. 2015;24(7):2011–22 [cited 2022 Jun 16]. Available from: https://pubmed.ncbi.nlm.nih.gov/25504048/.
29. Parvatiyar MS, Marshall JL, Nguyen RT, Jordan MC, Richardson VA, Roos KP, et al. Sarcospan regulates cardiac isoproterenol response and prevents Duchenne muscular dystrophy-associated cardiomyopathy. J Am Heart Assoc. 2015;4(12) [cited 2019 Nov 23]. Available from: http://www.ncbi.nlm.nih.gov/pubmed/26702077.
30. Gibbs EM, Marshall JL, Ma E, Nguyen TM, Hong G, Lam JS, et al. High levels of sarcospan are well tolerated and act as a sarcolemmal stabilizer to address skeletal muscle and pulmonary dysfunction in DMD. Hum Mol Genet. 2016;25(24):5395–406.
31. Parvatiyar MS, Brownstein AJ, Kanashiro-Takeuchi RM, Collado JR, Dieseldorff Jones KM, Gopal J, et al. Stabilization of the cardiac sarcolemma by sarcospan rescues DMD-associated cardiomyopathy. JCI insight. 2019:5 [cited 2019 May 7]. Available from: http://www.ncbi.nlm.nih.gov/pubmed/31039133.
32. Peter AK, Miller G, Crosbie RH. Disrupted mechanical stability of the dystrophin-glycoprotein complex causes severe muscular dystrophy in sarcospan transgenic mice. J Cell Sci. 2007;120(Pt 6):996–1008.
33. Yoshida-Moriguchi T, Campbell KP. Matriglycan: a novel polysaccharide that links dystroglycan to the basement membrane. Glycobiology. 2015;25(7):702–13 [cited 2022 Jun 16]. Available from: https://pubmed.ncbi.nlm.nih.gov/25882296/.
34. Holt KH, Lim LE, Straub V, Venzke DP, Duclos F, Anderson RD, et al. Functional rescue of the sarcoglycan complex in the BIO 14.6 hamster using delta-sarcoglycan gene transfer. Mol Cell. 1998;1(6):841–8 [cited 2022 Jun 16]. Available from: https://pubmed.ncbi.nlm.nih.gov/9660967/.
35. Marshall JL, Holmberg J, Chou E, Ocampo AC, Oh J, Lee J, et al. Sarcospan-dependent Akt activation is required for utrophin expression and muscle regeneration. J Cell Biol. 2012;197(7):1009–27 [cited 2019 Nov 23]. Available from: http://www.ncbi.nlm.nih.gov/pubmed/22734004.
36. Mamsa H, Stark RL, Shin KM, Beedle AM, Crosbie RH. Sarcospan increases laminin binding capacity of α-dystroglycan to ameliorate DMD independent of Galgt2. Hum Mol Genet. 2021;31(5):718-32.
37. Roberts TC, Johansson HJ, McClorey G, Godfrey C, Blomberg KEM, Coursindel T, et al. Multi-level omics analysis in a murine model of dystrophin loss and therapeutic restoration. Hum Mol Genet. 2015;24(23):6756–68.
38. Ge Y, Molloy MP, Chamberlain JS, Andrews PC. Differential expression of the skeletal muscle proteome in mdx mice at different ages. Electrophoresis. 2004;25(15):2576–85.
39. Matsumura CY, Menezes de Oliveira B, Durbeej M, Marques MJ. Isobaric tagging-based quantification for proteomic analysis: a comparative study of spared and affected muscles from mdx mice at the early phase of dystrophy. PLoS One. 2013;8(6):e65831.
40. Carberry S, Brinkmeier H, Zhang Y, Winkler CK, Ohlendieck K. Comparative proteomic profiling of soleus, extensor digitorum longus, flexor digitorum brevis and interosseus muscles from the mdx mouse model of Duchenne muscular dystrophy. Int J Mol Med. 2013;32(3):544–56.
41. Holland A, Henry M, Meleady P, Winkler CK, Krautwald M, Brinkmeier H, et al. Comparative label-free mass spectrometric analysis of mildly versus severely affected mdx mouse skeletal muscles identifies annexin, Lamin, and vimentin as universal dystrophic markers. Molecules. 2015;20(6):11317–44.
42. Murphy S, Zweyer M, Henry M, Meleady P, Mundegar RR, Swandulla D, et al. Label-free mass spectrometric analysis reveals complex changes in the brain proteome from the mdx-4cv mouse model of Duchenne muscular dystrophy. Clin Proteomics. 2015;12:27.
43. Murphy S, Zweyer M, Raucamp M, Henry M, Meleady P, Swandulla D, et al. Proteomic profiling of the mouse diaphragm and refined mass spectrometric analysis of the dystrophic phenotype. J Muscle Res Cell Motil. 2019;40(1):9–28.
44. Capitanio D, Moriggi M, Torretta E, Barbacini P, De Palma S, Viganò A, et al. Comparative proteomic analyses of Duchenne muscular dystrophy and Becker muscular dystrophy muscles: changes contributing to preserve muscle function in Becker muscular dystrophy patients. J Cachexia Sarcopenia Muscle. 2020;11(2):547–63 [cited 2020 Oct 22]. Available from: https://pubmed.ncbi.nlm.nih.gov/31991054/.
45. Dobin A, Davis CA, Schlesinger F, Drenkow J, Zaleski C, Jha S, et al. STAR: ultrafast universal RNA-seq aligner. Bioinformatics. 2013;29(1):15–21 [cited 2022 Jun 14]. Available from: https://pubmed.ncbi.nlm.nih.gov/23104886/.
46. Robinson MD, McCarthy DJ, Smyth GK. edgeR: a bioconductor package for differential expression analysis of digital gene expression data. Bioinformatics. 2010;26(1):139–40 [cited 2022 Jun 14]. Available from: https://pubmed.ncbi.nlm.nih.gov/19910308/.
47. Stearns-Reider KM, Hicks MR, Hammond KG, Reynolds JC, Maity A, Kurmangaliyev YZ, et al. Myoscaffolds reveal laminin scarring is detrimental for stem cell function while sarcospan induces compensatory fibrosis. bioRxiv. 2022:2022.07.07.497559 [cited 2022 Jul 8]. Available from: https://www.biorxiv.org/content/10.1101/2022.07.07.497559v1.
48. Barrett AS, Wither MJ, Hill RC, Dzieciatkowska M, D'Alessandro A, Reisz JA, et al. Hydroxylamine chemical digestion for insoluble extracellular matrix characterization. J Proteome Res. 2017;16(11):4177–84 [cited 2022 Jun 7]. Available from: https://pubmed.ncbi.nlm.nih.gov/28971683/.
49. Carberry S, Zweyer M, Swandulla D, Ohlendieck K. Proteomics reveals drastic increase of extracellular matrix proteins collagen and dermatopontin in the aged mdx diaphragm model of Duchenne muscular dystrophy. Int J Mol Med. 2012;30(2):229–34 [cited 2022 Jun 7]. Available from: https://pubmed.ncbi.nlm.nih.gov/22614334/.
50. Johnson TD, Hill RC, Dzieciatkowska M, Nigam V, Behfar A, Christman KL, et al. Quantification of decellularized human myocardial matrix: a comparison of six patients. Proteomics Clin Appl. 2016;10(1):75–83 [cited 2022 Jun 7]. Available from: https://pubmed.ncbi.nlm.nih.gov/26172914/.
51. Mi H, Ebert D, Muruganujan A, Mills C, Albou LP, Mushayamaha T, et al. PANTHER version 16: a revised family classification, tree-based classification tool, enhancer regions and extensive API. Nucleic Acids Res. 2021;49(D1):D394–403 [cited 2021 Dec 3]. Available from: https://academic.oup.com/nar/article/49/D1/D394/6027812.
52. Krämer A, Green J, Pollard JJ, Tugendreich S. Causal analysis approaches in ingenuity pathway analysis. Bioinformatics. 2014;30(4):523–30.
53. Calle EA, Hill RC, Leiby KL, Le AV, Gard AL, Madri JA, et al. Targeted proteomics effectively quantifies differences between native lung and detergent-decellularized lung extracellular matrices. Acta Biomater. 2016;46:91–100 [cited 2018 Mar 16]. Available from: http://www.ncbi.nlm.nih.gov/pubmed/27693690.
54. Nghiem PP, Hoffman EP, Mittal P, Brown KJ, Schatzberg SJ, Ghimbovschi S, et al. Sparing of the dystrophin-deficient cranial sartorius muscle is associated with classical and novel hypertrophy pathways in GRMD dogs. Am J Pathol. 2013;183(5):1411–24.
55. Duan R, Kim JH, Shilagardi K, Schiffhauer ES, Lee DM, Son S, et al. Spectrin is a mechanoresponsive protein shaping fusogenic synapse architecture during myoblast fusion. Nat Cell Biol. 2018;20(6):688–98 [cited 2022 Jun 16]. Available from: https://pubmed.ncbi.nlm.nih.gov/29802406/.
56. Deng H, Yang L, Wen P, Lei H, Blount P, Pan D. Spectrin couples cell shape, cortical tension, and hippo signaling in retinal epithelial morphogenesis. J Cell Biol. 2020;219(4) [cited 2022 Jun 16]. Available from: https://pubmed.ncbi.nlm.nih.gov/32328630/.
57. Cai X, Wang KC, Meng Z. Mechanoregulation of YAP and TAZ in cellular homeostasis and disease progression. Front Cell Dev Biol. 2021;9:1333.
58. Polesskaya A, Seale P, Rudnicki MA. Wnt signaling induces the myogenic specification of resident CD45+ adult stem cells during muscle regeneration. Cell. 2003;113(7):841–52 [cited 2022 Jun 7]. Available from: https://pubmed.ncbi.nlm.nih.gov/12837243/.

59. Eliazer S, Muncie JM, Christensen J, Sun X, D'Urso RS, Weaver VM, et al. Wnt4 from the niche controls the mechano-properties and quiescent state of muscle stem cells. Cell Stem Cell. 2019;25(5):654–665.e4 [cited 2022 Jun 7]. Available from: https://pubmed.ncbi.nlm.nih.gov/31495781/.
60. Gu Q, Tian H, Zhang K, Chen D, Chen D, Wang X, et al. Wnt5a/FZD4 mediates the mechanical stretch-induced osteogenic differentiation of bone mesenchymal stem cells. Cell Physiol Biochem. 2018;48(1):215–26 [cited 2022 Jun 7]. Available from: https://pubmed.ncbi.nlm.nih.gov/30007964/.
61. Kim KA, Wagle M, Tran K, Zhan X, Dixon MA, Liu S, et al. R-Spondin family members regulate the Wnt pathway by a common mechanism. Mol Biol Cell. 2008;19(6):2588–96 [cited 2022 Jun 7]. Available from: https://pubmed.ncbi.nlm.nih.gov/18400942/.
62. Han XH, Jin YR, Seto M, Yoon JK. A WNT/beta-catenin signaling activator, R-spondin, plays positive regulatory roles during skeletal myogenesis. J Biol Chem. 2011;286(12):10649–59 [cited 2022 Jun 7]. Available from: https://pubmed.ncbi.nlm.nih.gov/21252233/.
63. Lacour F, Vezin E, Bentzinger CF, Sincennes MC, Giordani L, Ferry A, et al. R-spondin1 controls muscle cell fusion through dual regulation of antagonistic Wnt signaling pathways. Cell Rep. 2017;18(10):2320–30 [cited 2022 Jun 7]. Available from: https://pubmed.ncbi.nlm.nih.gov/28273449/.
64. Schumacher S, Vazquez Nunez R, Biertümpfel C, Mizuno N. Bottom-up reconstitution of focal adhesion complexes. FEBS J. 2022;289(12) [cited 2022 Jun 29]. Available from: https://pubmed.ncbi.nlm.nih.gov/33999507/.
65. Mathiesen SB, Lunde M, Aronsen JM, Romaine A, Kaupang A, Martinsen M, et al. The cardiac syndecan-4 interactome reveals a role for syndecan-4 in nuclear translocation of muscle LIM protein (MLP). J Biol Chem. 2019;294(22):8717–31.
66. Han S, Cui C, Wang Y, He H, Liu Z, Shen X, et al. Knockdown of CSRP3 inhibits differentiation of chicken satellite cells by promoting TGF-β/Smad3 signaling. Gene. 2019;707:36–43 [cited 2022 Jun 29]. Available from: https://pubmed.ncbi.nlm.nih.gov/30930226/.
67. Raffaello A, Milan G, Masiero E, Carnio S, Lee D, Lanfranchi G, et al. JunB transcription factor maintains skeletal muscle mass and promotes hypertrophy. J Cell Biol. 2010;191(1):101–13 [cited 2022 Jun 7]. Available from: https://pubmed.ncbi.nlm.nih.gov/20921137/.
68. Nagakura R, Yamamoto M, Jeong J, Hinata N, Katori Y, Chang WJ, et al. Switching of Sox9 expression during musculoskeletal system development. Sci Rep. 2020;10(1) [cited 2022 Jun 7]. Available from: https://pubmed.ncbi.nlm.nih.gov/32439983/.
69. Bell DM, Leung KKH, Wheatley SC, Ng LJ, Zhou S, Ling KW, et al. SOX9 directly regulates the type-II collagen gene. Nat Genet. 1997;16(2):174–8 [cited 2022 Jun 7]. Available from: https://pubmed.ncbi.nlm.nih.gov/9171829/.
70. Iyer SR, Shah SB, Ward CW, Stains JP, Spangenburg EE, Folker ES, et al. Differential YAP nuclear signaling in healthy and dystrophic skeletal muscle. Am J Phys Cell Phys. 2019;317(1):C48–57 [cited 2022 Apr 14]. Available from: https://pubmed.ncbi.nlm.nih.gov/30995108/.
71. Wang Z, Yan N, Liu L, Cao D, Gao M, Lin C, et al. SOX9 overexpression plays a potential role in idiopathic congenital talipes equinovarus. Mol Med Rep. 2013;7(3):821–5.
72. Vong KI, Leung CKY, Behringer RR, Kwan KM. Sox9 is critical for suppression of neurogenesis but not initiation of gliogenesis in the cerebellum. Mol Brain. 2015;8:25.
73. Holland A, Ohlendieck K. Proteomic profiling of the dystrophin-deficient mdx phenocopy of dystrophinopathy-associated cardiomyopathy. Biomed Res Int. 2014;2014:246195 [cited 2017 Oct 23]. Available from: http://www.ncbi.nlm.nih.gov/pubmed/24772416.
74. Yokota T, McCourt J, Ma F, Ren S, Li S, Kim TH, et al. Type V collagen in scar tissue regulates the size of scar after heart injury. Cell. 2020;182(3):545–562.e23 [cited 2021 Jan 14]. Available from: https://pubmed.ncbi.nlm.nih.gov/32621799/.
75. Kühn K, Glanville RW, Babel W, Qian RQ, Dieringer H, Voss T, et al. The structure of type IV collagen. Ann N Y Acad Sci. 1985;460:14–24.
76. Wess TJ. Collagen fibril form and function. Adv Protein Chem. 2005;70:341–74.
77. Li A, Wei Y, Hung C, Vunjak-Novakovic G. Chondrogenic properties of collagen type XI, a component of cartilage extracellular matrix. Biomaterials. 2018;173:47–57.
78. Vázquez-Portalatı NN, Kilmer CE, Panitch A, Liu JC. Characterization of collagen type I and II blended hydrogels for articular cartilage tissue engineering. Biomacromolecules. 2016;17(10):3145–52.
79. Baghdadi MB, Castel D, Machado L, Fukada S-I, Birk DE, Relaix F, et al. Reciprocal signalling by notch-collagen V-CALCR retains muscle stem cells in their niche. Nature. 2018;557(7707):714–8.
80. Machnicka B, Grochowalska R, Bogusławska DM, Sikorski AF. The role of spectrin in cell adhesion and cell-cell contact. Exp Biol Med (Maywood). 2019;244(15):1303–12.
81. Pascual J, Pfuhl M, Walther D, Saraste M, Nilges M. Solution structure of the spectrin repeat: a left-handed antiparallel triple-helical coiled-coil. J Mol Biol. 1997;273(3):740–51.
82. Koenig M, Monaco AP, Kunkel LM. The complete sequence of dystrophin predicts a rod-shaped cytoskeletal protein. Cell. 1988;53(2):219–28.
83. Ayalon G, Hostettler JD, Hoffman J, Kizhatil K, Davis JQ, Bennett V. Ankyrin-B interactions with spectrin and dynactin-4 are required for dystrophin-based protection of skeletal muscle from exercise injury. J Biol Chem. 2011;286(9):7370–8.
84. Kerr JP, Robison P, Shi G, Bogush AI, Kempema AM, Hexum JK, et al. Detyrosinated microtubules modulate mechanotransduction in heart and skeletal muscle. Nat Commun. 2015;6:8526.
85. Tan N, Lansman JB. Utrophin regulates modal gating of mechanosensitive ion channels in dystrophic skeletal muscle. J Physiol. 2014;592(15):3303–23.
86. Khairallah RJ, Shi G, Sbrana F, Prosser BL, Borroto C, Mazaitis MJ, et al. Microtubules underlie dysfunction in duchenne muscular dystrophy. Sci Signal. 2012;5(236):ra56.
87. Suchyna TM, Sachs F. Mechanosensitive channel properties and membrane mechanics in mouse dystrophic myotubes. J Physiol. 2007;581(Pt 1):369–87.
88. Barton ER. Impact of sarcoglycan complex on mechanical signal transduction in murine skeletal muscle. Am J Phys Cell Phys. 2006;290(2):C411–9.
89. Kumar A, Khandelwal N, Malya R, Reid MB, Boriek AM. Loss of dystrophin causes aberrant mechanotransduction in skeletal muscle fibers. FASEB J Off Publ Fed Am Soc Exp Biol. 2004;18(1):102–13.
90. Schwartz MA, Shattil SJ. Signaling networks linking integrins and rho family GTPases. Trends Biochem Sci. 2000;25(8):388–91 [cited 2022 Jul 8]. Available from: https://pubmed.ncbi.nlm.nih.gov/10916159/.
91. Tejeda-Muñoz N, Morselli M, Moriyama Y, Sheladiya P, Pellegrini M, De Robertis EM. Canonical Wnt signaling induces focal adhesion and integrin beta-1 endocytosis. iScience. 2022;25(4) [cited 2022 Jul 8]. Available from: https://pubmed.ncbi.nlm.nih.gov/35402867/.
92. Wu X, Wang J, Jiang H, Hu Q, Chen J, Zhang J, et al. Wnt3a activates β1-integrin and regulates migration and adhesion of vascular smooth muscle cells. Mol Med Rep. 2014;9(4):1159–64 [cited 2022 Jul 8]. Available from: https://pubmed.ncbi.nlm.nih.gov/24535659/.
93. Lawson CD, Burridge K. The on-off relationship of rho and Rac during integrin-mediated adhesion and cell migration. Small GTPases. 2014;5(MAR) [cited 2022 Jul 8]. Available from: https://pubmed.ncbi.nlm.nih.gov/24607953/.
94. Clark EA, King WG, Brugge JS, Symons M, Hynes RO. Integrin-mediated signals regulated by members of the rho family of GTPases. J Cell Biol. 1998;142(2):573–86 [cited 2022 Jul 8]; Available from: https://pubmed.ncbi.nlm.nih.gov/9679153/.
95. Miki H, Suetsugu S, Takenawa T. WAVE, a novel WASP-family protein involved in actin reorganization induced by Rac. EMBO J. 1998;17(23):6932–41 [cited 2022 Jun 7]. Available from: https://pubmed.ncbi.nlm.nih.gov/9843499/.
96. Young P, Ehler E, Gautel M. Obscurin, a giant sarcomeric rho guanine nucleotide exchange factor protein involved in sarcomere assembly. J Cell Biol. 2001;154(1):123–36 [cited 2022 Jun 7]. Available from: https://pubmed.ncbi.nlm.nih.gov/11448995/.
97. Ford-Speelman DL, Roche JA, Bowman AL, Bloch RJ. The rho-guanine nucleotide exchange factor domain of obscurin activates rhoA signaling in skeletal muscle. Mol Biol Cell. 2009;20(17):3905–17 [cited 2022 Jun 7]. Available from: https://pubmed.ncbi.nlm.nih.gov/19605563/.

98. Li X, Matsuoka Y, Bennett V. Adducin preferentially recruits spectrin to the fast growing ends of actin filaments in a complex requiring the MARCKS-related domain and a newly defined oligomerization domain. J Biol Chem. 1998;273(30):19329–38 [cited 2022 Jun 7]. Available from: https://pubmed.ncbi.nlm.nih.gov/9668123/.
99. Hughes CA, Bennett V. Adducin: a physical model with implications for function in assembly of spectrin-actin complexes. J Biol Chem. 1995;270(32):18990–6 [cited 2022 Jun 7]. Available from: https://pubmed.ncbi.nlm.nih.gov/7642559/.
100. Oak SA, Zhou YW, Jarrett HW. Skeletal muscle signaling pathway through the dystrophin glycoprotein complex and Rac1. J Biol Chem. 2003;278(41):39287–95 [cited 2022 Jun 7]. Available from: https://pubmed.ncbi.nlm.nih.gov/12885773/.
101. Hill CS, Wynne J, Treisman R. The rho family GTPases RhoA, Rac1, and CDC42Hs regulate transcriptional activation by SRF. Cell. 1995;81(7):1159–70 [cited 2022 Jun 7]. Available from: https://pubmed.ncbi.nlm.nih.gov/7600583/.

Publisher's Note